Published by
NIGERIAN SOCIETY OF PHYSICAL SCIENCES
Available online @ https://journal.nsps.org.ng/index.php/jnsps

J. Nig. Soc. Phys. Sci. 8 (2026) 3397

Journal of the Nigerian Society of Physical Sciences

Optimal control of smoking-induced asthma and cardiovascular disorders with medical and public health interventions

Muhammad Farman[a,b,c,*], Noreen Asghar[d], Muhammad Umer Saleem[d], Nezihal Gokbulut[a], Evren Hincal[a,e], Aseel Smerat[f,g], Mohamed Hafez[h,i]

[a]Faculty of Arts and Sciences, Department of Mathematics, Near East University, Mersin-10, Turkey
[b]Faculty of Medicine, Department of Biostatistics and Medical Informatics, Karadeniz Technical University, Trabzon, Turkey
[c]International Center for Interdisciplinary Research in Sciences, The University of Lahore, Lahore, 54600, Pakistan
[d]Department of Mathematics, University of Education, Lahore, 54600, Pakistan
[e]Research Center of Applied Mathematics, Khazar University, Baku, AZ1096, Azerbaijan
[f]Faculty of Educational Sciences, Al-Ahliyya Amman University, Amman 19328, Jordan
[g]Department of Biosciences, Saveetha School of Engineering, Saveetha Institute of Medical and Technical Sciences, Chennai, 602105, India
[h]Faculty of Engineering and Quantity Surveying, INTI International University Colleges, 71800, Nilai, Malaysia
[i]Faculty of Management, Shinawatra University, Pathum Thani, 12000, Thailand

Abstract

Smoking is a major public health concern because of its harmful effects on several organs and its association with respiratory and cardiovascular complications. Cardiovascular disease is more common among smokers, and awareness of smoking cessation is important for reducing smoking prevalence. In this study, a compartmental model is developed to analyze the effect of awareness on the control of smoking and smoking-induced asthma and cardiovascular disorders. The positively invariant region, boundedness, positivity, and other basic dynamical properties of the model are established. Equilibria are obtained, and local and global stability analyses are performed. The normalized forward sensitivity index is used to assess the influence of key parameters on smoking cessation. Numerical simulations are conducted using a reliable nonstandard finite difference (NSFD) method. The simulation results show that smoking substantially increases the risk of respiratory and cardiovascular illnesses and that intervention strategies can reduce disease severity and prevalence. The model is further extended to an optimal-control framework that emphasizes the importance of treatment implementation and public awareness in reducing smoking-related harm. The results highlight the importance of media-based awareness and the need to inform potential smokers about the dangers of smoking. The proposed mathematical framework can support policymakers and health professionals in designing targeted interventions to reduce tobacco and cigarette use.

DOI: 10.46481/jnsps.2026.3397

Keywords: Cardiovascular disease modeling, Optimal control, Nonstandard finite difference (NSFD), Public health interventions

Article History:
Received: 30 March 2026
Received in revised form: 27 June 2026
Accepted for publication: 28 June 2026
Available online: 27 July 2026

Communicated by: B. J. Falaye

1. Introduction

The increasing death rate of tobacco users worldwide indicates that tobacco use is becoming a serious addiction that needs to be managed. Smoking must be viewed as a significant global issue in order to stop the development of smoking habits.

*Corresponding author Tel. No.: +905391318241.
Email address: farmanlink@gmail.com (Muhammad Farman)

The management of smoking addiction is greatly influenced by the media. It increases public knowledge of the negative consequences of smoking [1]. Asthma is a long-term respiratory condition that causes recurring episodes of wheezing, coughing, chest tightness, and shortness of breath by constricting and inflaming the airways. Even so, there is currently no viable long-term treatment for total elimination. Toxic irritants like ammonia, acrolein, and nitrogen oxides are introduced into the respiratory system by tobacco smoke, which impairs lung function and increases vulnerability to asthma triggers [2–4]. Millions of children worldwide are exposed to secondhand smoke on a daily basis, and many of them already have exacerbated asthma disorders as a result of passive inhalation [5, 6]. The burden of asthma in vulnerable populations is further increased by other airborne pollutants, such as dust from mining operations, heavy metal particles from industrial combustion, and emissions from refineries [7–9].

A potent method for examining the dynamics of these chronic illnesses and offering insights into measures for control and prevention is mathematical modeling [10–13]. From fractional-order systems to deterministic compartmental models, a variety of modeling approaches have been used to study respiratory and smoking-related disorders [14–17]. Several studies have modeled smoking dynamics to examine how the model compartments interacted with one another. Castillo-Garsow *et al.* [18] presented the most basic system to represent such dynamics in 1997. Later, in 2008, the mathematical equation for temporarily quitting smokers was expanded to include another compartment [19]. A methodical framework for developing tactics that balance intervention costs and reduce illness burden is provided by optimal control. Verma [20] examined a nonlinear smoking model with control variables, emphasizing how awareness efforts can lower the prevalence of smoking. While Zaman *et al.* [21] investigated treatment optimization in epidemic models with time delay, Ref. [22] used optimal control to examine intervention options in drinking populations.

A fractional optimal control model was developed to examine HIV/TB co-infection dynamics, where sensitivity analysis and optimal intervention strategies were employed to reduce disease prevalence and transmission burden [23]. Similarly, Caputo fractional-order approaches have been utilized to study HIV/HCV co-infection dynamics by incorporating memory-dependent effects, stability analysis, and numerical simulations to better understand long-term disease progression and treatment behavior [24]. In more recent times, Zakary *et al.* [25] expanded these methods to multi-regional epidemic scenarios and Refs. [26, 27] applied optimal control to alcohol-related health models. Refs. [28–30] presented the best ways to prevent the spread of diseases like COVID-19, dengue, and Zika in the setting of co-infections by combining vaccination and awareness campaigns. Together, these studies demonstrate that the predictive ability and policy relevance of mathematical models are greatly enhanced by the inclusion of control mechanisms like treatment and awareness.

An analysis of the effects of tobacco use on the prevalence of tuberculosis is presented, including an optimum control study. Faniran *et al.* [31] present a study on related ideas. In Ref. [32], the authors explored a smoking cessation model with a media campaign. Disseminating information to encourage smokers to stop was therefore a beneficial intervention. To control the spread of smoking in society, the authors of Ref. [33] first created a deterministic model and then expanded it to a stochastic model. To find the optimal control approach for a discrete mathematical model of smoking with a specific saturation incidence rate, the author of Ref. [34] examined three control strategies: awareness programs, treatment, and psychological support. It was found that a program of education might significantly lower the number of smokers [35]. In order to reduce tobacco use in a population, the author of Ref. [36] created a mathematical model that is further extended to an optimum control problem by taking into account three control strategies, such as education campaigns, anti-nicotine gum, and anti-nicotine. To examine the dynamics of smoking behavior, the authors of Ref. [37] looked into a mathematical model. They used education campaigns, a government ban on smoking in public areas, and higher cigarette costs as control measures to lower the number of smokers. The characterization of optimal controls is examined using Pontryagin's Maximum Principle.

Although considerable progress has been made in fractional and optimal control modeling of infectious and treatment-related diseases, limited attention has been devoted to smoking-induced asthma and cardiovascular complications under combined medical and public health intervention strategies. There is a gap in models that incorporate smoking-induced asthma transmission and cardiac illnesses with public health interventions because existing works frequently concentrate on cancer or broad respiratory problems. In order to address this, we provide a unique deterministic model that takes into account various smoking classes and investigates their contribution to the progression of blood pressure and asthma. In the present study, the proposed smoking-induced asthma and cardiovascular disorder model is formulated within the classical integer-order framework. The primary objective of this work is to investigate the qualitative dynamics, optimal control strategies, and chaotic behavior of the coupled system using standard differential equations. Since the considered epidemiological interactions and control mechanisms can be effectively described through classical derivatives, the integer-order formulation was considered sufficient and mathematically appropriate for the present analysis. The basic reproductive number, equilibrium points, boundedness, and well-posedness of the model are examined. Sensitivity analysis is used to determine the main factors influencing the prevalence of asthma. To further lessen the burden of asthma and heart diseases, two ideal control measures are introduced: medical interventions and awareness efforts. The results highlight the impact of medical services and public health initiatives in reducing disease prevalence and show how important smoking reduction is in preventing the spread of heart disease and asthma.

The work is organized as follows: Section 1 in this article serves as an introduction. Normalized sensitivity analysis, equilibrium points, and well-posedness are all included in the recently developed model in Section 2. Section 3 verifies the model's existence and uniqueness. Section 4 presents the

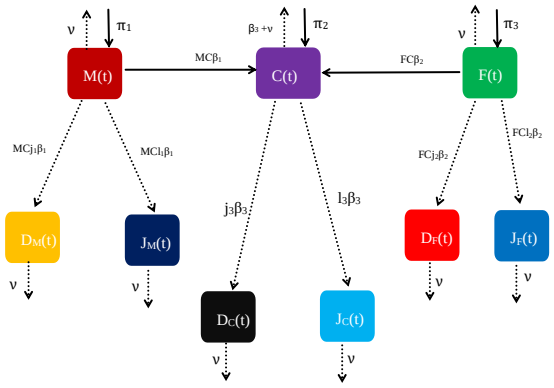

Figure 1: Flow chart of the dynamical system.

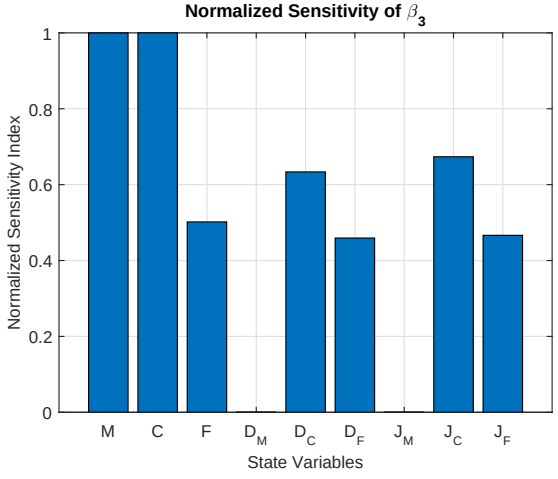

Figure 2: Normalized sensitivity indices of system compartments with respect to β_3.

stability analysis of the proposed model. We examine the numerical scheme in Section 5 using nonstandard finite difference (NSFD) techniques and convergence analysis. In Section 6, we develop the optimal-control strategies using control parameters and their control results. Section 7 discusses the conclusion and future directions of the proposed public health paradigm.

The figures and tables supporting the model formulation, sensitivity analysis, numerical validation, and optimal-control simulations are presented in Figures 1- 21, and Tables 1 and 2.

2. Formulation of the dynamical model for smoking-induced asthma and high blood pressure

In this work, we develop a mathematical model describing the interaction between smoking dynamics and smoking-induced asthma and cardiovascular disorders. The total population is partitioned into three distinct smoking-status compartments:

- $M(t)$: Non-smoker individuals;

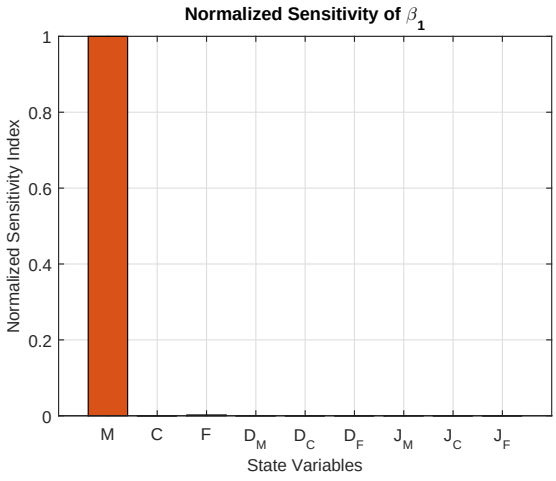

Figure 3: Normalized sensitivity indices of system compartments with respect to β_1.

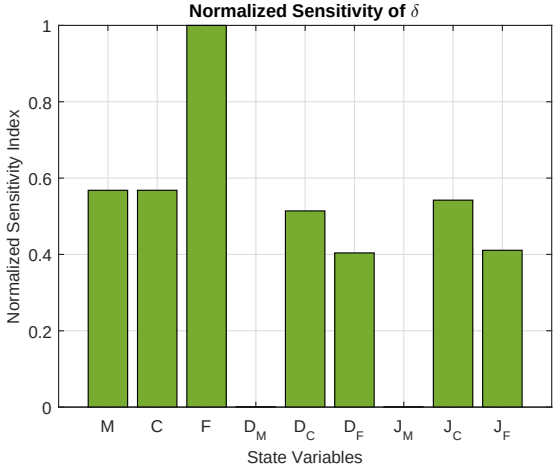

Figure 4: Normalized sensitivity indices of system compartments with respect to δ.

Table 1: Normalized sensitivity indices of the principal model parameters.

State Variable	β_1	β_3	δ
M	1.0000	1.0000	0.5681
C	0.0000	1.0000	0.5681
F	0.0021	0.5018	1.0000
D_M	0.0001	0.0002	0.0001
D_C	0.0000	0.6337	0.5141
D_F	0.0000	0.4592	0.4040
J_M	0.0002	0.0002	0.0001
J_C	0.0000	0.6734	0.5422
J_F	0.0000	0.4665	0.4109

- $C(t)$: Active-smoker individuals; and
- $F(t)$: Ex-smoker individuals.

To capture the prevalence of smoking-induced asthma and car-

Table 2: Descriptions of parameters of the model.

Symbols	Descriptions	Overall	Women/Men	Unit	Reference
M	Non-smoker individuals	1339	860 / 479	Individuals	TRNC
C	Active-smoker individuals	863	303 / 560	Individuals	TRNC
F	Ex-smoker individuals	345	128 / 217	Individuals	TRNC
D_M	Non-smokers with asthma	50	39 / 11	Individuals	TRNC
D_C	Active-smokers with asthma	22	9 / 13	Individuals	TRNC
D_F	Ex-smokers with asthma	12	8 / 4	Individuals	TRNC
J_M	Non-smokers with heart disease	58	31 / 27	Individuals	TRNC
J_C	Active-smokers with heart disease	40	18 / 22	Individuals	TRNC
J_F	Ex-smokers with heart disease	30	6 / 24	Individuals	TRNC
π_1	Recruitment rate for non-smokers	600	660 / 380	Individuals/year	TRNC
π_2	Recruitment rate for active-smokers	400	234 / 450	Individuals/year	TRNC
π_3	Recruitment rate for ex-smokers	160	99 / 170	Individuals/year	TRNC
β_1	Second-hand smoking rate (M(t))	0.575	0.583 / 0.56	$year^{-1}$	[39]
β_2	Second-hand smoking rate (C(t))	0.683	0.8 / 0.75	$year^{-1}$	[39]
β_3	Second-hand smoking rate (F(t))	0.77	0.62 / 0.65	$year^{-1}$	[39]
ν	Natural death rate	0.0002	0.0002 / 0.0002	$year^{-1}$	[39]
δ	Awareness rate	0.514	0.546 / 0.48	$year^{-1}$	[39]
j_1	Control parameter	0.04	0.046 / 0.024	Dimensionless	Assumed
j_2	Control parameter	0.024	0.066 / 0.019	Dimensionless	Assumed
j_3	Control parameter	0.027	0.03 / 0.024	Dimensionless	Assumed
l_1	Control parameter	0.044	0.04 / 0.058	Dimensionless	Assumed
l_2	Control parameter	0.018	0.05 / 0.011	Dimensionless	Assumed
l_3	Control parameter	0.048	0.06 / 0.041	Dimensionless	Assumed

diovascular diseases, we further introduce disease-related sub-populations within each smoking-status class. The following disease-related sub-populations represent individuals suffering from asthma or cardiovascular complications within each smoking-status class:

- $D_M(t)$: Non-smoker individuals with bronchitis or asthma;
- $D_C(t)$: Active smoker individuals with bronchitis or asthma;
- $D_F(t)$: Ex-smoker individuals with bronchitis or asthma;
- $J_M(t)$: Non-smoker individuals with heart diseases or high blood pressure;
- $J_C(t)$: Active smoker individuals with heart diseases or high blood pressure; and
- J_F(t): Ex-smoker individuals with heart diseases or high blood pressure.

It is important to emphasize that the variables $D_M, D_C, D_F, J_M, J_C,$ and J_F represent disease-prevalence sub-populations. These variables correspond to living individuals who suffer from asthma or cardiovascular disorders within the respective smoking-status classes. Therefore, natural mortality acts on these sub-populations through the rate ν. The disease-prevalence compartments are overlapping with the primary smoking-status classes $M(t), C(t)$, and $F(t)$. They are introduced to quantify the prevalence of smoking-related health complications and do not alter the total smoking-status dynamics.

2.1. Assumptions

- Through recruiting, the class of non-smokers $M(t)$ grows at a rate π_1. Interaction with active smokers can expose nonsmokers to secondhand smoke at a rate β_1, which increases the risk of heart disease and asthma. Every member of this class passes away naturally at a rate ν. Consequently, at time t we have

$$\frac{dM}{dt} = \pi_1 - \beta_1 MC - \nu M. \tag{1}$$

- Through recruiting, the active-smoker class C expands at a rate π_2. People in this class may transfer to the ex-smoker class at a rate δ if they decide to stop smoking owing to awareness or educational willingness. Active smokers experience natural mortality at a rate ν and disease progression due to smoke exposure at a rate β_3. So,

$$\frac{dC}{dt} = \pi_2 - \beta_3 C - \delta C - \nu C. \tag{2}$$

- Due to recruitment at rate π_3 and the transition of current smokers quitting at rate δ, the ex-smoker class $F(t)$ grows. Ex-smokers may still be exposed to smoking surroundings, which increases their risk of developing heart disease or asthma at a rate of $\beta_2 FC$. They also die naturally at a rate ν, much like other groups. Consequently,

$$\frac{dF}{dt} = \pi_3 + \delta C - \beta_2 FC - \nu F. \tag{3}$$

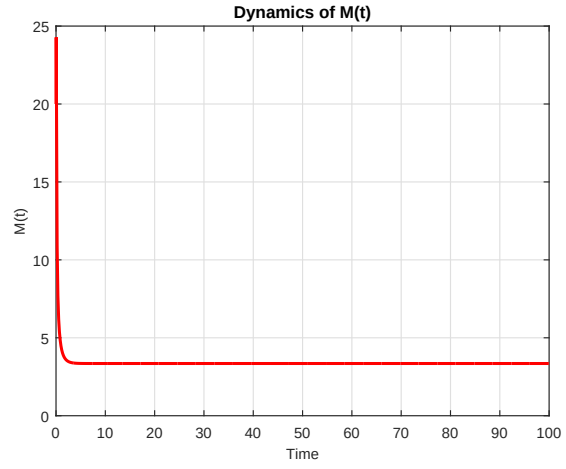

(a)

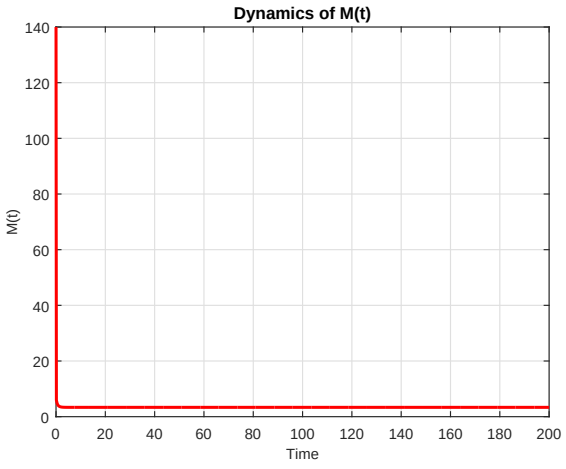

(b)

Figure 5: The dynamical behavior of Non-smokers M(t) under different initial conditions.

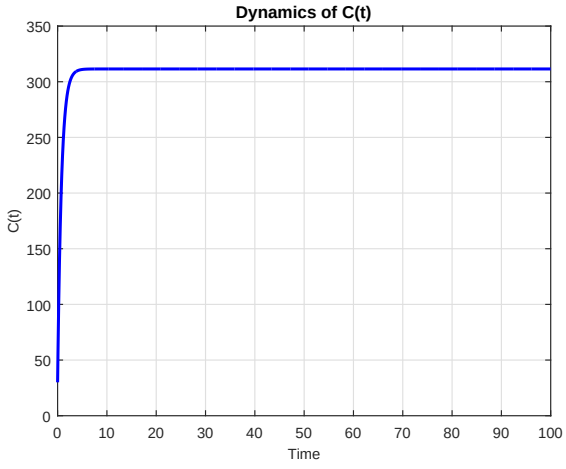

(a)

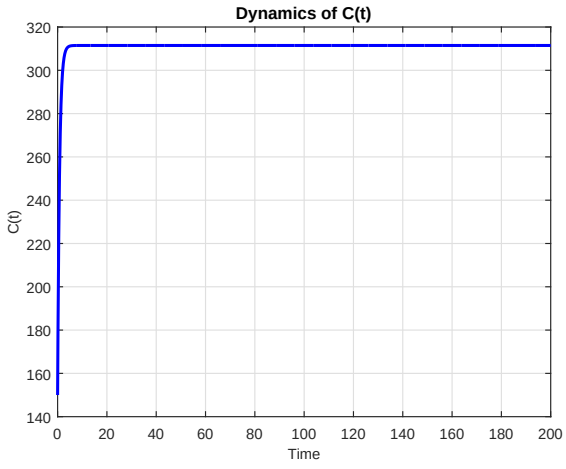

(b)

Figure 6: The dynamical behavior of Active-smokers C(t) under different initial conditions.

- The quantity $D_M(t)$ represents the prevalence of smoking-induced asthma cases observed among non-smokers exposed to second-hand smoke. New asthma cases arise at rate $j_1\beta_1 MC$, while individuals are removed through natural mortality at rate ν. Thus,

$$\frac{dD_M}{dt} = j_1\beta_1 MC - \nu D_M. \tag{4}$$

- The compartment $D_C(t)$ represents the prevalence of smoking-induced asthma cases among active smokers. New cases occur at rate $j_3\beta_3 C$, while natural mortality removes individuals at rate ν. Hence,

$$\frac{dD_C}{dt} = j_3\beta_3 C - \nu D_C. \tag{5}$$

- The class $D_F(t)$ represents the prevalence of smoking-induced asthma cases among ex-smokers. New asthma cases arise at rate $j_2\beta_2 FC$, while natural death occurs at rate ν. Consequently,

$$\frac{dD_F}{dt} = j_2\beta_2 FC - \nu D_F. \tag{6}$$

- The quantity $J_M(t)$ represents the prevalence of smoking-induced cardiovascular disease observed among non-smokers who are exposed to second-hand smoke. New heart disease cases arise at rate $l_1\beta_1 MC$, while individuals in this compartment are removed through natural mortality at rate ν. Hence:

$$\frac{dJ_M}{dt} = l_1\beta_1 MC - \nu J_M. \tag{7}$$

- The class $J_C(t)$ represents the prevalence of cardiovascular disease among active smokers. New cases develop at rate $l_3\beta_3 C$, while natural death removes individuals at rate ν. Thus:

$$\frac{dJ_C}{dt} = l_3\beta_3 C - \nu J_C. \tag{8}$$

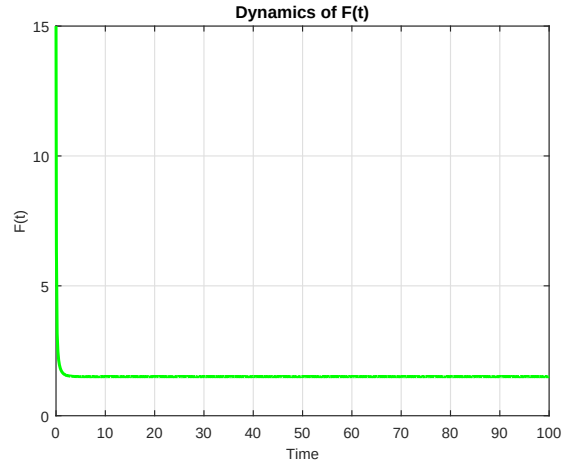

(a)

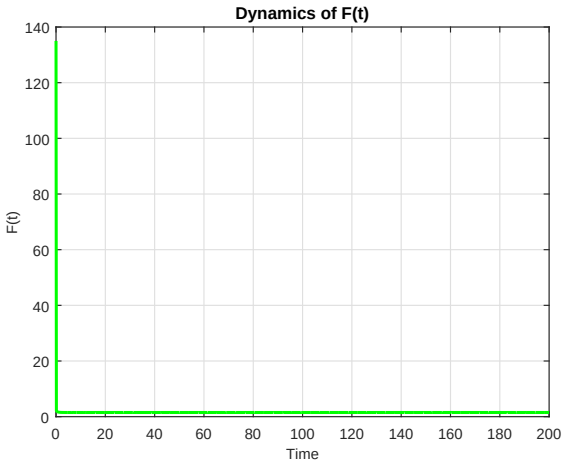

(b)

Figure 7: The dynamical behavior of Ex-smokers F(t) under different initial conditions.

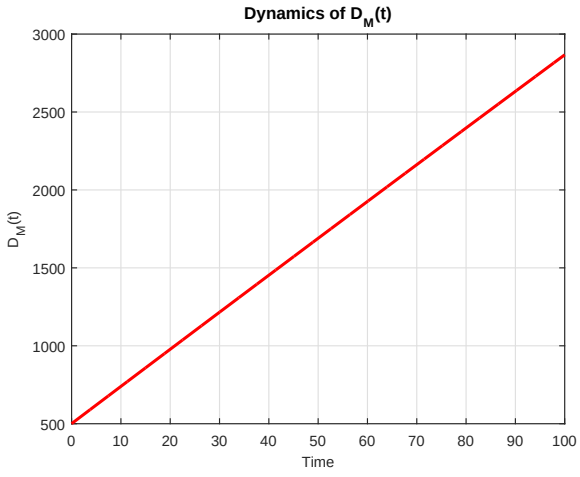

(a)

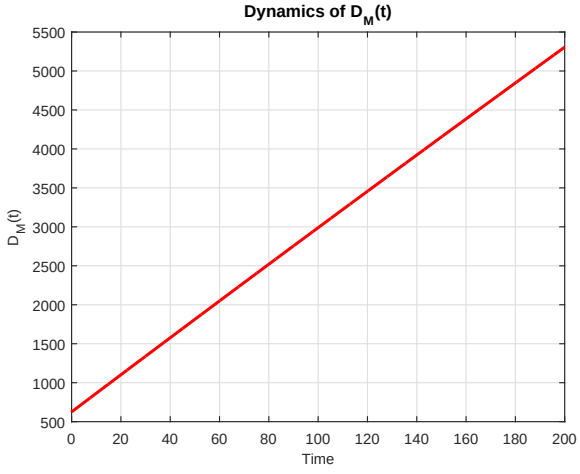

(b)

Figure 8: The dynamical behavior of $D_M(t)$ under different initial conditions.

- The compartment $J_F(t)$ represents the prevalence of cardiovascular disease among ex-smokers who previously had smoking exposure. New cases occur at rate $l_2\beta_2 FC$, and individuals leave the compartment due to natural mortality at rate ν. Therefore,

$$\frac{dJ_F}{dt} = l_2\beta_2 FC - \nu J_F. \tag{9}$$

2.2. Development of asthma disease model

In classical modeling using ordinary differential equations, the rate of change of a variable depends only on its current state. The current model is developed using a system of ODEs in which explicit transition factors that indicate smoking behavior and illness progression control the rate of change of each compartment. The disease-prevalence compartments quantify the number of individuals suffering from smoking-related asthma and cardiovascular complications within each smoking-status class. The system's deterministic evolution over time is captured by the ODE framework. This formulation offers an analytically manageable depiction of how smoking affects people's transition from healthy to ill states.

$$\begin{aligned}
\frac{dM}{dt} &= \pi_1 - \beta_1 MC - \nu M,\\
\frac{dC}{dt} &= \pi_2 - \beta_3 C - \delta C - \nu C,\\
\frac{dF}{dt} &= \pi_3 + \delta C - \beta_2 FC - \nu F,\\
\frac{dD_M}{dt} &= j_1\beta_1 MC - \nu D_M,\\
\frac{dD_C}{dt} &= j_3\beta_3 C - \nu D_C,\\
\frac{dD_F}{dt} &= j_2\beta_2 FC - \nu D_F,\\
\frac{dJ_M}{dt} &= l_1\beta_1 MC - \nu J_M,\\
\frac{dJ_C}{dt} &= l_3\beta_3 C - \nu J_C,\\
\frac{dJ_F}{dt} &= l_2\beta_2 FC - \nu J_F,
\end{aligned} \tag{10}$$

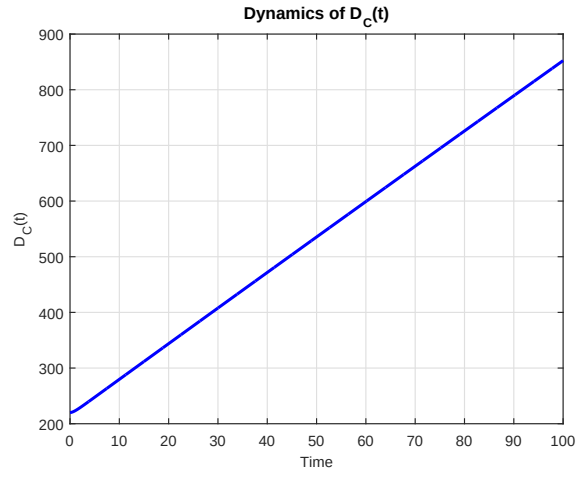

(a)

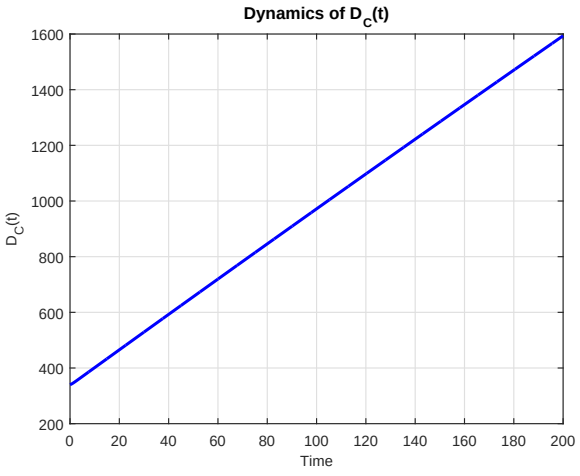

(b)

Figure 9: The dynamical behavior of $D_C(t)$ under different initial conditions.

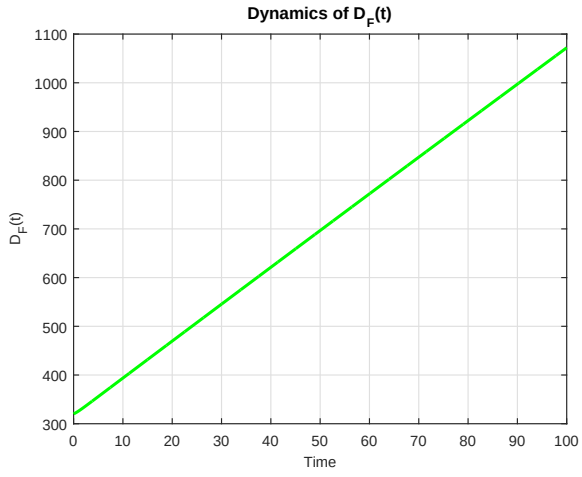

(a)

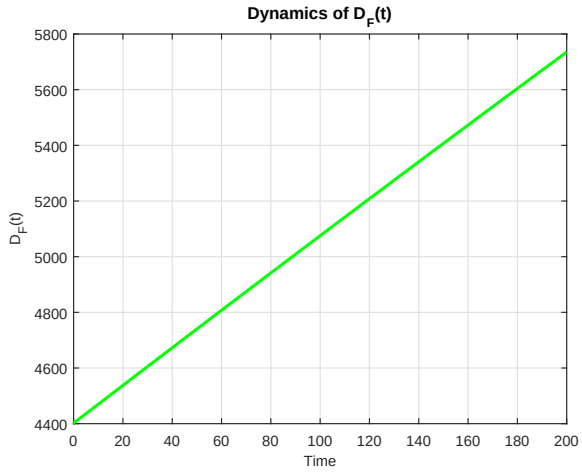

(b)

Figure 10: The dynamical behavior of $D_F(t)$ under different initial conditions.

with the initial conditions

$$M(0) \geq 0,\ C(0) \geq 0,\ F(0) \geq 0,\ D_M(0) \geq 0,\ D_C(0) \geq 0,$$
$$D_F(0) \geq 0,\ J_M(0) \geq 0,\ J_C(0) \geq 0,\ J_F(0) \geq 0.$$

The new smoking-induced asthma and heart disease flow chart model that we developed for this study is shown in Figure 1.

2.3. *Positively invariant region*

Lemma 1. According to Ref. [38], every system in the region $\Xi \in \mathbb{R}^9_+$

$$\Xi = \{(M, C, F, D_M, D_C, D_F, J_M, J_C, J_F) \in \mathbb{R}^9_+ : 0 \leq \aleph\}$$

attracts the solution to the system (in equation) (10), and under positive initial conditions, it remains positively invariant for the chosen system in $\mathbb{R}^9_+$.

Proof. We will write about the systems' positive solutions (10) and provide the following results:

$$\frac{dM}{dt}|_{M=0} = \pi_1 \geq 0,$$
$$\frac{dC}{dt}|_{C=0} = \pi_2 \geq 0,$$
$$\frac{dF}{dt}|_{F=0} = \pi_3 + \delta C \geq 0,$$
$$\frac{dD_M}{dt}|_{D_M=0} = j_1\beta_1 MC \geq 0,$$
$$\frac{dD_C}{dt}|_{D_C=0} = j_3\beta_3 C \geq 0,$$
$$\frac{dD_F}{dt}|_{D_F=0} = j_2\beta_2 FC \geq 0,$$
$$\frac{dJ_M}{dt}|_{J_M=0} = l_1\beta_1 MC \geq 0,$$
$$\frac{dJ_C}{dt}|_{J_C=0} = l_3\beta_3 C \geq 0,$$

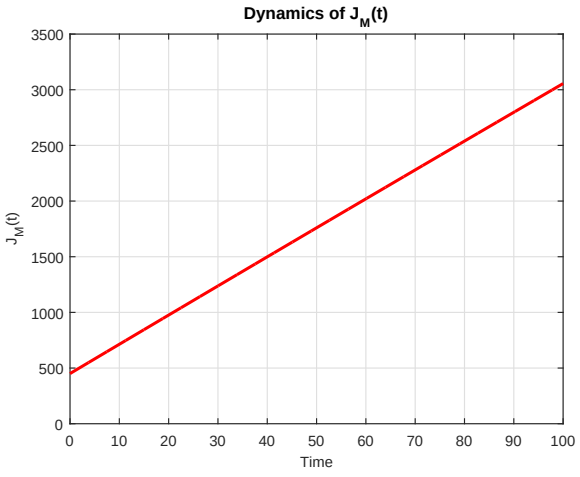

(a)

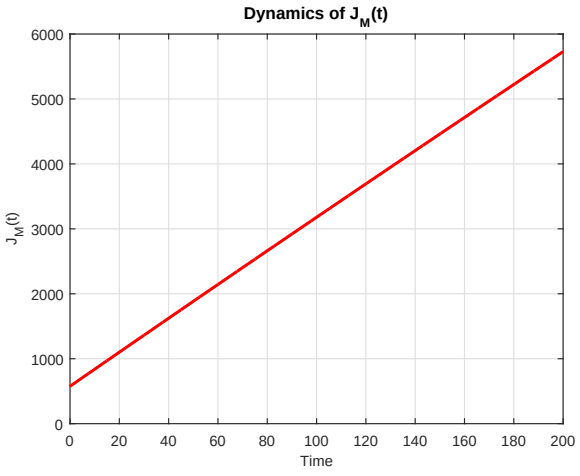

(b)

Figure 11: The dynamical behavior of $J_M(t)$ under different initial conditions.

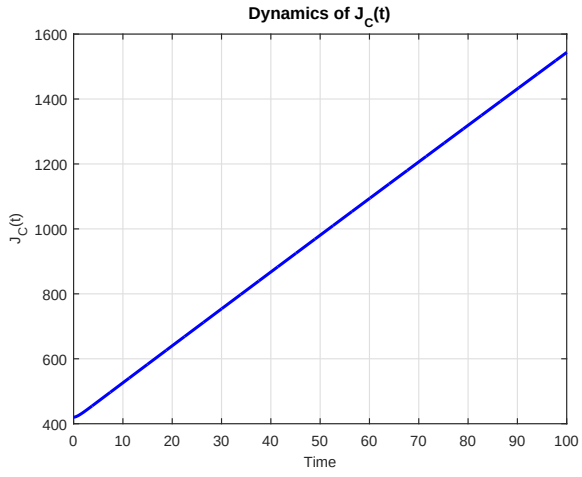

(a)

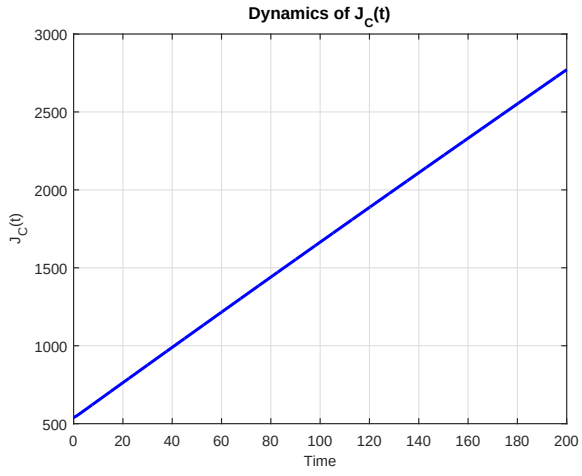

(b)

Figure 12: The dynamical behavior of $J_C(t)$ under different initial conditions.

$$\frac{dJ_F}{dt}\,|_{J_F=0} = l_2\beta_2 FC \geq 0. \tag{11}$$

As per the system (11), if $t \geq 0$, the vector field appears to be situated on every hyperplane in the domain $\mathbb{R}^9_+$ that contains the non-negative orthant. □

2.4. Equilibrium points

The equilibrium states of the proposed model (10) are as follows:

$$E^0 = \left(M^0,\ C^0,\ F^0,\ D_M^0,\ D_C^0,\ D_F^0,\ J_M^0,\ J_C^0,\ J_F^0\right)$$

$$= \left(\frac{\pi_1}{\nu}, 0, \frac{\pi_3}{\nu}, 0, 0, 0, 0, 0, 0\right).$$

$$E^* = (M^*, C^*, F^*, D_M^*, D_C^*, D_F^*, J_M^*, J_C^*, J_F^*),$$

where

$$M^* = \frac{\pi_1}{\beta_1 C^* + \nu}, \quad D_M^* = \frac{j_1\beta_1 M^* C^*}{\nu}, \quad J_M^* = \frac{l_1\beta_1 M^* C^*}{\nu},$$

$$C^* = \frac{\pi_2}{\beta_3 + \delta + \nu}, \quad D_C^* = \frac{j_3\beta_3 C^*}{\nu}, \quad J_C^* = \frac{l_3\beta_3 C^*}{\nu},$$

$$F^* = \frac{\pi_3 + \delta C^*}{\beta_2 C^* + \nu}, \quad D_F^* = \frac{j_2\beta_2 F^* C^*}{\nu}, \quad J_F^* = \frac{l_2\beta_2 F^* C^*}{\nu}.$$

The equilibrium state E^0 represents the baseline steady-state of the smoking-status populations before the occurrence of smoking-induced asthma and cardiovascular disease. At this equilibrium, all disease-prevalence compartments are zero, indicating the absence of disease prevalence, while the smoking-status populations remain at their equilibrium levels.

2.5. Normalized sensitivity analysis

We conducted a sensitivity analysis as in Ref. [39] by introducing tiny perturbations around the baseline value $\beta_3 = 0.77; \beta_1 = 0.575;$ and $\delta = 0.514$ in order to evaluate the impact of β_3, β_1 and δ on the system dynamics. Figures 2-4 summarizes the normalized sensitivity indices for $M(t), C(t), F(t), D_M(t), D_C(t), D_F(t), J_M(t), J_C(t), J_F(t)$.

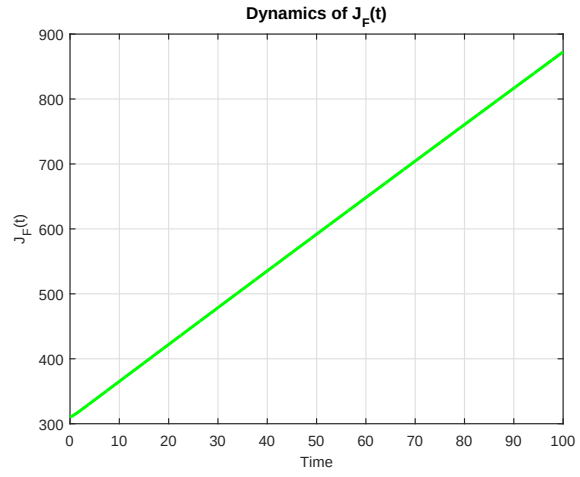

(a)

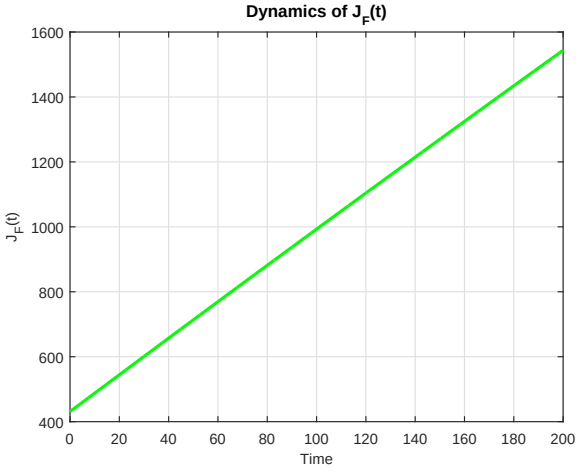

(b)

Figure 13: The dynamical behavior of $J_F(t)$ under different initial conditions.

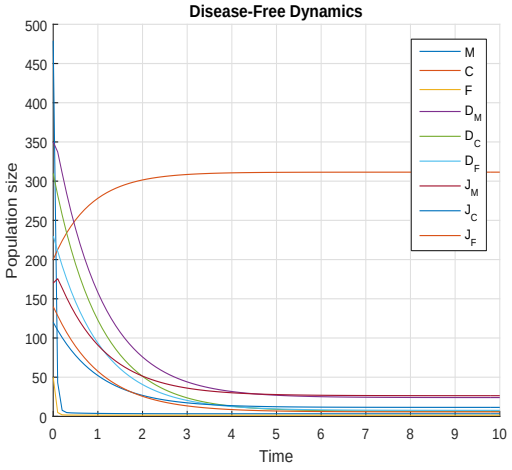

Figure 14: Numerical simulation of the proposed NSFD scheme for baseline smoking equilibrium (BSE).

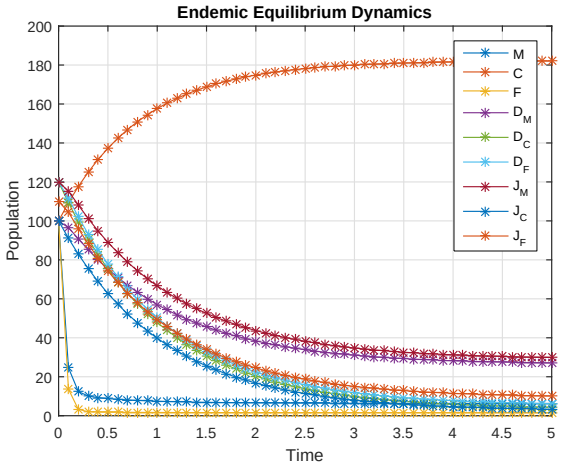

(a)

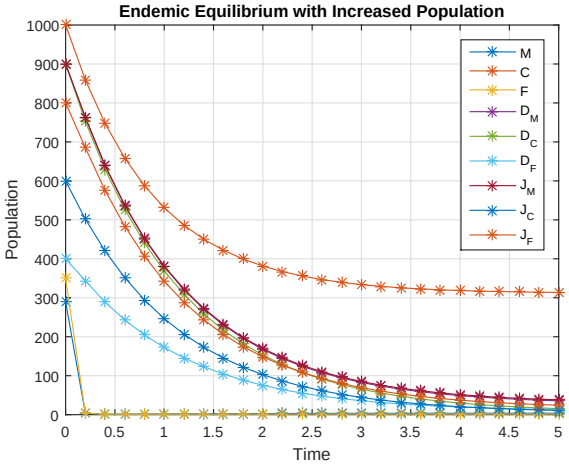

(b)

Figure 15: Numerical simulations for PE under different initial population sizes.

Table 1 presents the normalized sensitivity indices of the selected model parameters. The results indicate that the second-hand smoke exposure parameter β_1 exerts its strongest influence on the non-smoker population M. In contrast, the smoking progression parameter β_3 has the greatest impact on the active smoker population and the associated disease compartments, particularly D_C and J_C. Furthermore, the smoking cessation parameter δ exhibits the highest sensitivity with respect to the ex-smoker population F and substantially affects the disease prevalence among former smokers. These findings suggest that smoking progression and cessation mechanisms play a dominant role in shaping the dynamics of smoking-induced asthma and cardiovascular disorders.

3. Existence and uniqueness analysis

Let $\mathbf{Y}(t) = (M, C, F, D_M, D_C, D_F, J_M, J_C, J_F)^T$ represent the system (10)'s state vector as in Ref. [39]. The compact form of

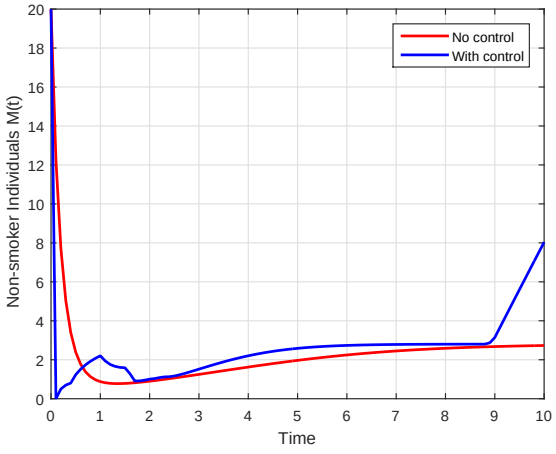

(a)

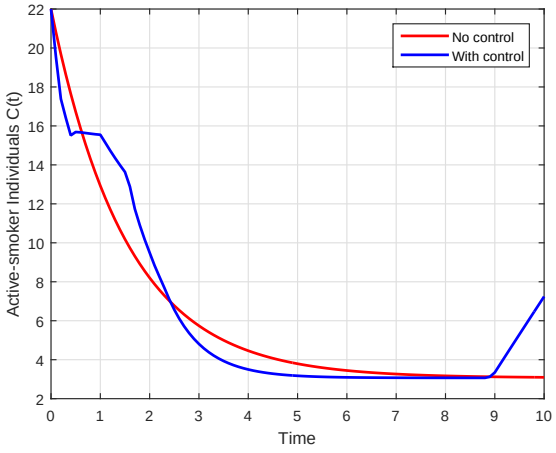

(b)

Figure 16: Individual dynamics with and without control measures for M(t) and C(t).

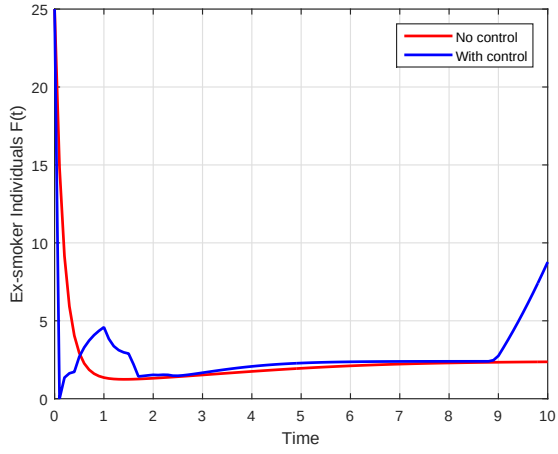

(a)

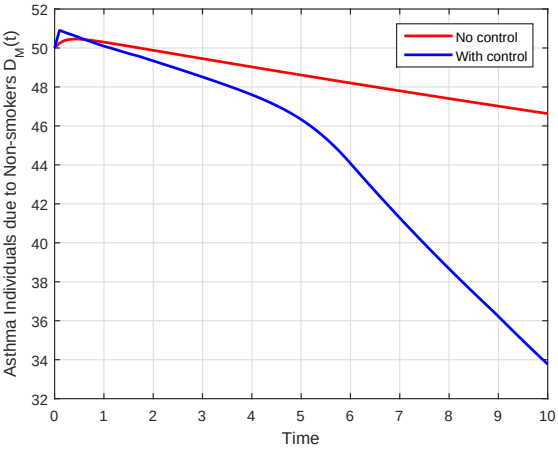

(b)

Figure 17: Individual dynamics with and without control measures for F(t) and $D_M(t)$.

the model can then be written:

$$\frac{d\mathbf{Y}}{dt} = \mathbf{H}(t, \mathbf{Y}), \quad Y(0) = Y_0, \tag{12}$$

where $\mathbf{H} = (H_1, H_2, \ldots, H_9)^T$ is the nonlinear vector function that corresponds to the system's right side (10).
We must confirm that the function $\mathbf{H}(t, \mathbf{Y})$ fulfills both the Lipschitz and linear growth conditions in order to prove the existence of solutions.

(1.) $\mid H_j(t, M, C, F, D_M, D_C, D_F, J_M, J_C, J_F) \mid^2 \leq G_j(1+ \mid M \mid^2)$, $j = 1, 2, \ldots, 9$.

(2.) $\forall M, M_1, \ \| H(t, M, \omega) - H(t, M_1, \omega) \|_\infty^2 \leq \tilde{G}_j \| M - M_1 \|_\infty^2$, with $\omega = (C, F, D_M, D_C, D_F, J_M, J_C, J_F)$.

We first confirm that the growth condition is linear. Examine the first part of the nonlinear function $\mathbf{H}$: then $\mid \varnothing_1(\varpi_1) \mid^2 \leq T_1 \left(1+ \mid M \mid^2\right)$,

$$|H_1(\varpi_1)|^2 = |\pi_1 - (\beta_1 C + \nu)M|^2.$$

By applying the triangle inequality and the parameters' boundedness, we arrive at

$$|H_1(\varpi_1)|^2 \leq 2\pi_1^2 + 2(\beta_1 C + \nu)^2 \mid M \mid^2 .$$

Hence,

$$|H_1(\varpi_1)|^2 \leq 2\pi_1^2 \left(1 + \frac{(\beta_1 C + \nu)^2 \mid M \mid^2}{\pi_1^2}\right).$$

If $\left(\frac{(\beta_1 C+\nu)^2 |M|^2}{\pi_1^2}\right) < 1$, with $G_1 = 2\pi_1^2$, then

$$|H_1(\varpi_1)|^2 \leq G_1(1 + |M|^2).$$

Analogous constraints can be obtained for the remaining components H_i, $i = 2, 3, ..., 9$. Consequently, there is a positive constant $\mathbf{G} > 0$ such that:

$$\|\mathbf{H}(t, \mathbf{Y})\|^2 \leq \mathbf{G}(1 + \|\mathbf{Y}\|^2),$$

where the linear growth criterion is verified by a constant $\mathbf{G} > 0$ that depends on the model parameters. The Lipschitz condition

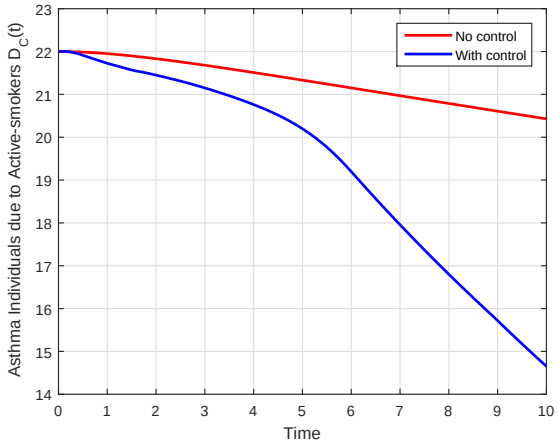

(a)

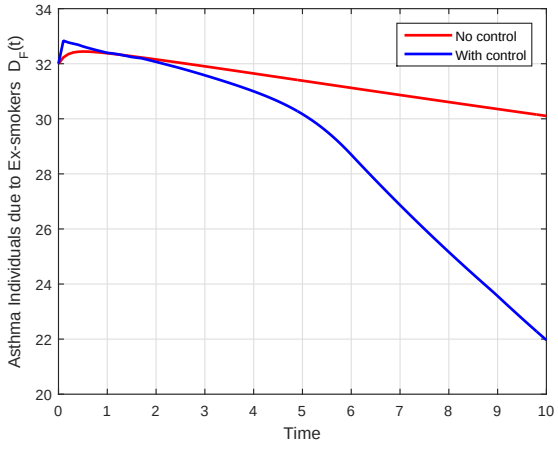

(b)

Figure 18: Individual dynamics with and without control measures in the $D_C(t)$ and $D_F(t)$.

for the nonlinear function $\mathbf{H}$ is therefore confirmed. Consider the first element:

$$\begin{aligned}
&|H_1(t, M, C, F, D_M, D_C, D_F, J_M, J_C, J_F) \\
&- H_1(t, M^1, C, F, D_M, D_C, D_F, J_M, J_C, J_F)|^2 \\
&=| \pi_1 - \beta_1 MC - \nu M - (\pi_1 - \beta_1 M^1 C - \nu M^1) \,|^2 \\
&= |(\beta_1 C + \nu)(M - M^1)|^2 \leq (\beta_1 C + \nu)^2 |M - M^1|^2.
\end{aligned} \tag{13}$$

By taking supremum over $t \in D_M$, we get

$$\begin{aligned}
&\sup_{t \in D_M} |H_1(t, M, C, F, D_M, D_C, D_F, J_M, J_C, J_F) \\
&\quad - H_1(t, M^1, C, F, D_M, D_C, D_F, J_M, J_C, J_F)\Big|^2 \\
&\leq (\beta_1 C + \nu)^2 \sup_{t \in D_M} |M - M^1|^2.
\end{aligned}$$

$$\begin{aligned}
&\sup_{t \in D_M} |H_1(t, M, C, F, D_M, D_C, D_F, J_M, J_C, J_F) \\
&\quad - H_1(t, M^1, C, F, D_M, D_C, D_F, J_M, J_C, J_F)\Big|^2 \\
&\leq (\beta_1 C + \nu)^2 \, \|M - M^1\|_\infty^2.
\end{aligned}$$

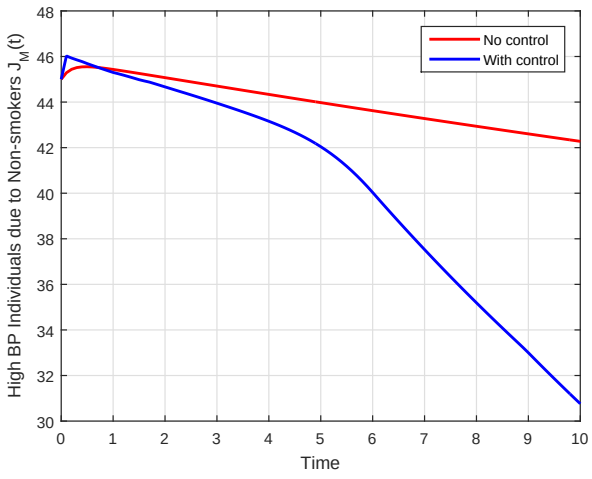

(a)

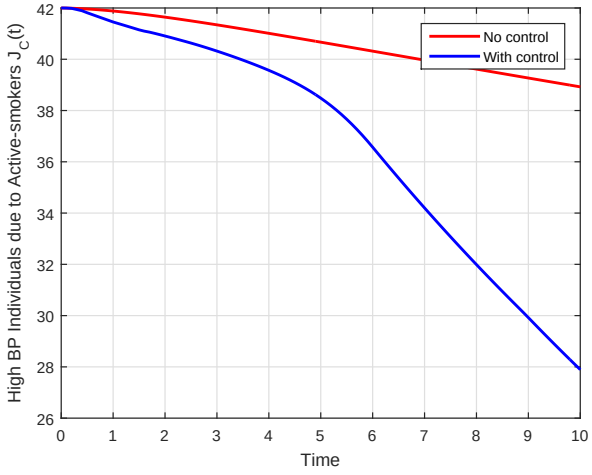

(b)

Figure 19: Dynamics of individuals in the $J_M(t)$ and $J_C(t)$ with and without control measures.

Let $\bar{G}_1 = (\beta_1 C + \nu)^2$, then

$$|H_1(t, Y) - H_1(t, Y_1)|^2 \leq \bar{G}_1 \|M - M^1\|_\infty^2.$$

Analogous inequalities are also satisfied by the remaining components H_i, $i = 2, 3, ..., 9$. Consequently, there is a constant $\mathbf{K} > 0$ such that:

$$\|\mathbf{H}(t, \mathbf{Y}) - \mathbf{H}(t, \mathbf{Y}_1)\| \leq \mathbf{K} \|\mathbf{Y} - \mathbf{Y}_1\|,$$

for all $\mathbf{Y}, \mathbf{Y}_1 \in \mathbb{R}^9$, where $\mathbf{K} > 0$ is a Lipschitz constant. Therefore, the Lipschitz condition is satisfied by the function $\mathbf{H}(t, \mathbf{Y})$. Consequently, the Lipschitz and linear growth criteria are satisfied by the function $\mathbf{H}(t, \mathbf{Y})$.

According to the Picard–Lindelöf theorem, the system (10) has a unique solution under the following condition:

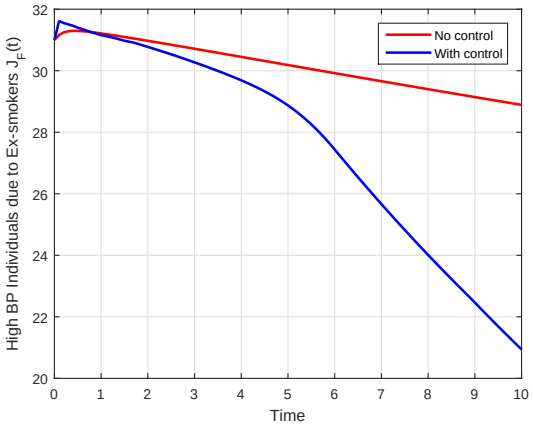

Figure 20: Dynamics of individuals in $J_F(t)$ with and without control measures.

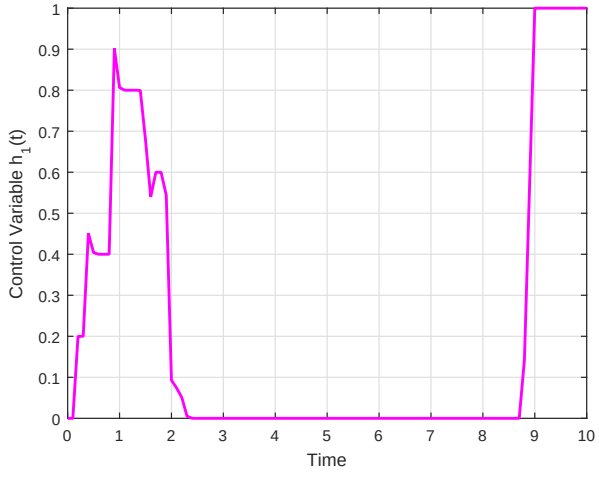

(a)

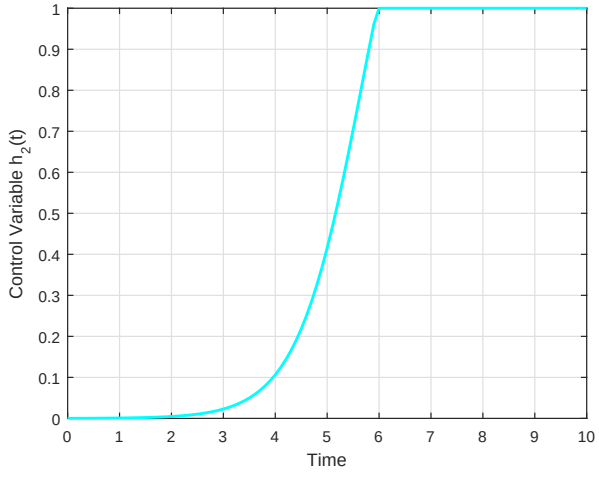

(b)

Figure 21: Dynamics of the control variables $\hbar_1(t)$ and $\hbar_2(t)$.

$$\max\left\{\begin{array}{l}\dfrac{(\beta_1 C+\nu)^2 \mid M \mid^2}{\pi_1^2}\\ \dfrac{(\beta_3+\delta+\nu)^2 \mid C \mid^2}{\pi_2^2}\\ \dfrac{(\beta_2 \mid C \mid^2+\nu)^2 \mid F \mid^2}{(\pi_3^2+\delta^2 \mid C \mid^2)}\\ \dfrac{\nu^2 \mid D_M \mid^2}{(j_1^2\beta_1^2 \mid M \mid^2 \mid C \mid^2)}\\ \dfrac{\nu^2 \mid D_C \mid^2}{(j_3^2\beta_3^2 \mid C \mid^2)}\\ \dfrac{\nu^2 \mid D_F \mid^2}{(j_2^2\beta_2^2 \mid F \mid^2 \mid C \mid^2)}\\ \dfrac{\nu^2 \mid J_M \mid^2}{(l_1^2\beta_1^2 \mid M \mid^2 \mid C \mid^2)}\\ \dfrac{\nu^2 \mid J_C \mid^2}{(l_3^2\beta_3^2 \mid C \mid^2)}\\ \dfrac{\nu^2 \mid J_F \mid^2}{(l_2^2\beta_2^2 \mid F \mid^2 \mid C \mid^2)}\end{array}\right. < 1. \tag{14}$$

In conclusion, the research above shows that the model's right side meets Lipschitz-type and standard growth conditions. Therefore, the proposed (10) system admits a unique solution that exists for the considered time span for any physiologically valid beginning population values. This ensures that the model is well-posed mathematically. From a modeling standpoint, this guarantees the validity of the system dynamics and the significance and reproducibility of numerical simulations.

4. Local stability analysis

Theorem 4.1. Let E^0 denote the baseline smoking equilibrium of system (10). According to Ref. [39], the equilibrium point E^0 is locally asymptotically stable if all eigenvalues of the Jacobian matrix $J(E^0)$ have negative real parts.

Proof. Jacobian matrix for the system (10) at E°, can be expressed as:

$$J(E^\circ)=\begin{bmatrix}-(\beta_1C^*+\nu) & -\beta_1M^* & 0 & 0 & 0 & 0 & 0 & 0 & 0\\ 0 & -(\beta_3+\delta+\nu) & 0 & 0 & 0 & 0 & 0 & 0 & 0\\ 0 & \delta-\beta_2F^* & -\beta_2C^*-\nu & 0 & 0 & 0 & 0 & 0 & 0\\ j_1\beta_1C^* & j_1\beta_1M^* & 0 & -\nu & 0 & 0 & 0 & 0 & 0\\ 0 & j_3\beta_3 & 0 & 0 & -\nu & 0 & 0 & 0 & 0\\ 0 & j_2\beta_2F^* & j_2\beta_2C^* & 0 & 0 & -\nu & 0 & 0 & 0\\ l_1\beta_1C^* & l_1\beta_1M^* & 0 & 0 & 0 & 0 & -\nu & 0 & 0\\ 0 & l_3\beta_3 & 0 & 0 & 0 & 0 & 0 & -\nu & 0\\ 0 & l_2\beta_2F^* & l_2\beta_2C^* & 0 & 0 & 0 & 0 & 0 & -\nu\end{bmatrix}.$$

Furthermore, the calculated characteristic roots are as follows:

$$\lambda_1=-0.0002,\ \lambda_2=-0.0002,\ \lambda_3=-496.2252,\ \lambda_4=-0.0002,$$

$$\lambda_5=-0.0002,\ \lambda_6=-589.4292,\ \lambda_7=-0.0002,$$

$$\lambda_8=-0.0002,\ \lambda_9=-1.2842.$$

Since all computed eigenvalues of the Jacobian matrix evaluated at E^0 possess strictly negative real parts, the equilibrium point E^0 satisfies the local asymptotic stability criterion established by Ref. [39]. Therefore, for the parameter values listed in Table 2, the baseline smoking equilibrium E^0 is locally asymptotically stable. □

The dynamical behavior of all compartments under different initial conditions is displayed in Figures 5-13.

The left column represents simulations over the time interval ($0 \le t \le 100$), while the right column shows the behavior for a longer time horizon ($0 \le t \le 200$). The results demonstrate that the system trajectories approach consistent bounded patterns despite different initial conditions. The theoretical analysis guarantees that small perturbations in the system or in the initial conditions lead only to small deviations in the system trajectories. In other words, the approximate solutions remain close to the exact solutions within a bounded region. Although the compartments exhibit transient fluctuations and oscillatory behavior, all trajectories remain bounded and eventually approach stable patterns over time.

4.1. Global stability analysis

Theorem 4.2. Let E^* denote the positive equilibrium of system (10). If there exists a continuously differentiable Lyapunov function $\mathcal{L}$ such that

$$\mathcal{L}(E^*) = 0, \quad \mathcal{L} > 0 \quad \text{for} \quad E \neq E^*, \quad \text{and} \quad \dot{\mathcal{L}} \le 0$$

throughout the feasible region, then the positive equilibrium E^* is globally asymptotically stable according to LaSalle's invariance principle.

Proof. The following is an expression for the Lyapunov function:

$$\mathcal{L} = \sum_{X \in \{M,C,F,D_M,D_C,D_F,J_M,J_C,J_F\}} \left(X - X^* - X^* \ln \frac{X}{X^*}\right). \tag{15}$$

$$\begin{aligned}\mathcal{L}(M^*, C^*, F^*, D_M^*, D_C^*, D_F^*, J_M^*, J_C^*, J_F^*) &= \left(M - M^* - M^* \ln \frac{M^*}{M}\right) \\ &+ \left(C - C^* - C^* \ln \frac{C^*}{C}\right) + \left(F - F^* - F^* \ln \frac{F^*}{F}\right) \\ &+ \left(D_M - D_M^* - D_M^* \ln \frac{D_M^*}{D_M}\right) + \left(D_C - D_C^* - D_C^* \ln \frac{D_C^*}{D_C}\right) \\ &+ \left(D_F - D_F^* - D_F^* \ln \frac{D_F^*}{D_F}\right) + \left(J_M - J_M^* - J_M^* \ln \frac{J_M^*}{J_M}\right) \\ &+ \left(J_C - J_C^* - J_C^* \ln \frac{J_C^*}{J_C}\right) + \left(J_F - J_F^* - J_F^* \ln \frac{J_F^*}{J_F}\right). \end{aligned} \tag{16}$$

Since $X > 0$, we use the standard inequality:

$$x - 1 \ge \ln x \quad \text{for all } x > 0, \tag{17}$$

which implies

$$X - X^* - X^* \ln \frac{X}{X^*} \ge 0. \tag{18}$$

Thus, $\mathcal{L}$ is positive definite and $\mathcal{L} = 0$ only at E^*. Now differentiating $\mathcal{L}$ along system trajectories gives:

$$\frac{d\mathcal{L}}{dt} = \sum \left(1 - \frac{X^*}{X}\right) \frac{dX}{dt}. \tag{19}$$

Substituting the model equations, we obtain:

$$\begin{aligned}\frac{d\mathcal{L}}{dt} &= \left(\frac{M - M^*}{M}\right)(\pi_1 - \beta_1 MC - \nu M) + \left(\frac{C - C^*}{C}\right) \\ &(\pi_2 - \beta_3 C - \delta C - \nu C) + \left(\frac{F - F^*}{F}\right)(\pi_3 + \delta C - \beta_2 FC - \nu F) \\ &+ \left(\frac{D_M - D_M^*}{D_M}\right)(j_1\beta_1 MC - \nu D_M) + \left(\frac{D_C - D_C^*}{D_C}\right) \\ &(j_3\beta_3 C - \nu D_C) + \left(\frac{D_F - D_F^*}{D_F}\right)(j_2\beta_2 FC - \nu D_F) \\ &+ \left(\frac{J_M - J_M^*}{J_M}\right)(l_1\beta_1 MC - \nu J_M) + \left(\frac{J_C - J_C^*}{J_C}\right)(l_3\beta_3 C - \nu J_C) \\ &+ \left(\frac{J_F - J_F^*}{J_F}\right)(l_2\beta_2 FC - \nu J_F). \end{aligned} \tag{20}$$

Now we apply the standard logarithmic inequality $1 - \frac{X^*}{X} \le \ln \frac{X}{X^*}$, and also use the positivity of all state variables. Using this inequality, and replacing $M = M - M^*$, $C = C - C^*$, $F = F - F^*$, $D_M = D_M - D_M^*$, $D_C = D_C - D_C^*$, $D_F = D_F - D_F^*$, $J_M = J_M - J_M^*$, $J_C = J_C - J_C^*$, $J_F = J_F - J_F^*$. Following certain calculations, we can have the following $\frac{d\mathcal{L}}{dt}$ to reduce complexity:

$$\frac{d\mathcal{L}}{dt} \le \Phi_1 - \Phi_2,$$

$$\begin{aligned}\Phi_1 &= \pi_1 + (\beta_1 C + \nu)M^* + \pi_2 + (\beta_3 + \delta + \nu)C^* + (\pi_3 + \delta C) \\ &+ (\beta_2 C + \nu)F^* + j_1\beta_1 MC + \nu D_M^* + j_3\beta_3 C + \nu D_C^* + \nu J_F^* \\ &+ j_2\beta_2 FC + \nu D_F^* + l_1\beta_1 MC + \nu J_M^* + l_3\beta_3 C + \nu J_C^* + l_2\beta_2 FC, \end{aligned} \tag{21}$$

$$\begin{aligned}\Phi_2 &= \pi_1\left(\frac{M^*}{M}\right) + (\beta_1 C + \nu)M + \pi_2\left(\frac{C^*}{C}\right) + (\beta_3 + \delta + \nu)C \\ &+ (\pi_3 + \delta C)\left(\frac{F^*}{F}\right) + (\beta_2 C + \nu)F + j_1\beta_1 MC\left(\frac{D_M^*}{D_M}\right) + \nu D_M \\ &+ j_3\beta_3 C\left(\frac{D_C^*}{D_C}\right) + \nu D_C + j_2\beta_2 FC(\frac{D_F^*}{D_F}) + \nu D_F + l_1\beta_1 MC\left(\frac{J_M^*}{J_M}\right) \\ &+ \nu J_M + l_3\beta_3 C\left(\frac{J_C^*}{J_C}\right) + \nu J_C + l_2\beta_2 FC\left(\frac{J_F^*}{J_F}\right) + \nu J_F. \end{aligned} \tag{22}$$

The implication is that $\frac{d\mathcal{L}}{dt} < 0$ if $\Phi_1 < \Phi_2$ for every point in the feasible region. Conversely, with $M = M^*$, $C = C^*$, $F = F^*$, $D_M = D_M^*$, $D_C = D_C^*$, $D_F = D_F^*$, $J_M = J_M^*$, $J_C = J_C^*$, and $J_F = J_F^*$, we obtain

$$0 = \Phi_1 - \Phi_2 \quad \Rightarrow \quad \frac{d\mathcal{L}}{dt} = 0. \tag{23}$$

Therefore, the largest invariant subset of $\{\frac{d\mathcal{L}}{dt} = 0\}$ consists only of the equilibrium E^*. Consequently, by LaSalle's invariance

principle, the positive equilibrium point E^* is globally asymptotically stable. For positive population states, the logarithmic structure of the Lyapunov function remains well-defined and gives a relative measure of each population compartment's departure. □

5. Numerical algorithm and validation of the suggested approach

The objective of this section is to provide a mathematical framework that replicates the system's continuous model dynamics, as demonstrated by the set of equations (10). We can determine that $h = \Delta t > 0$ is a step size using the criterion stated in Ref. [40] and the results of Anguelov and Lubuma.

$$\begin{aligned}
\frac{M^{k+1}-M^k}{\varphi} &= \pi_1 - \beta_1 M^{k+1}C^k - \nu M^{k+1},\\
\frac{C^{k+1}-C^k}{\varphi} &= \pi_2 - \beta_3 C^{k+1} - \delta C^{k+1} - \nu C^{k+1},\\
\frac{F^{k+1}-F^k}{\varphi} &= \pi_3 + \delta C^{k+1} - \beta_2 F^{k+1}C^{k+1} - \nu F^{k+1},\\
\frac{D_M^{k+1}-D_M^k}{\varphi} &= j_1\beta_1 M^{k+1}C^{k+1} - \nu D_M^{k+1},\\
\frac{D_C^{k+1}-D_C^k}{\varphi} &= j_3\beta_3 C^{k+1} - \nu D_C^{k+1},\\
\frac{D_F^{k+1}-D_F^k}{\varphi} &= j_2\beta_2 F^{k+1}C^{k+1} - \nu D_F^{k+1},\\
\frac{J_M^{k+1}-J_M^k}{\varphi} &= l_1\beta_1 M^{k+1}C^{k+1} - \nu J_M^{k+1},\\
\frac{J_C^{k+1}-J_C^k}{\varphi} &= l_3\beta_3 C^{k+1} - \nu J_C^{k+1},\\
\frac{J_F^{k+1}-J_F^k}{\varphi} &= l_2\beta_2 F^{k+1}C^{k+1} - \nu J_F^{k+1},
\end{aligned} \tag{24}$$

The suggested NSFD Scheme for the specified model is as follows:

$$\varphi = \frac{1-e^{-n^*h}}{n^*}, \tag{25}$$

with $n^* = \max\{(\beta_1 C+\nu), (\beta_3+\delta+\nu), (\beta_2 C+\nu), (\nu)\}$. As stated by Ref. [41], the discrete method (24) is categorized as an NSFD approach based on Mickens' criterion. This technique is developed using the method described by Anguelov and Lubuma in Ref. [40].

(Rule 1:) Equation (24) replaces the conventional denominator $h = \Delta$ of the discrete derivatives with the complex denominator function $\varphi(h) = h + O(h^2)$. This substitution serves to ensure that the denominator function φ of the continuous model accurately represents the dynamics of the system. According to studies by Lubuma and Patidar in 2007 and Gumel in Ref. [42, 43], exact techniques using such intricate denominator operations are applied in a variety of dynamical systems.

(Rule 2:) The nonlinear variables are incorporated into the right side of the system of equations via the non-local approximation (10). For instance, we have $C(t_k)F(t_k) \cong C_{k+1}F_k$ rather than $C(t_k)F(t_k) \cong C_kF_k$.

5.1. Analysis of suggested novel scheme

Theorem 5.1. The continuous model system described by the system of equations (10) includes the NSFD scheme (24) inside the physiologically viable domain k.

Proof. We have:

$$\begin{aligned}
M^{k+1} &= \frac{M^k+\varphi(\pi_1)}{1+\varphi(\beta_1 C^k+\nu)},\\
C^{k+1} &= \frac{C^k+\varphi(\pi_2)}{1+\varphi(\beta_3+\delta+\nu)},\\
F^{k+1} &= \frac{F^k+\varphi(\pi_3+\delta C^{k+1})}{1+\varphi(\beta_2 C^{k+1}+\nu)},\\
D_M^{k+1} &= \frac{D_M^k+\varphi(j_1\beta_1 M^{k+1}C^{k+1})}{1+\varphi\nu},\\
D_C^{k+1} &= \frac{D_C^k+\varphi(j_3\beta_3 C^{k+1})}{1+\varphi\nu},\\
D_F^{k+1} &= \frac{D_F^k+\varphi(j_2\beta_2 F^{k+1}C^{k+1})}{1+\varphi\nu},\\
J_M^{k+1} &= \frac{J_M^k+\varphi(l_1\beta_1 M^{k+1}C^{k+1})}{1+\varphi\nu},\\
J_C^{k+1} &= \frac{J_C^k+\varphi(l_3\beta_3 C^{k+1})}{1+\varphi\nu},\\
J_F^{k+1} &= \frac{J_F^k+\varphi(l_2\beta_2 F^{k+1}C^{k+1})}{1+\varphi\nu},
\end{aligned} \tag{26}$$

$M^{k+1} \geq 0$, $C^{k+1} \geq 0$, $F^{k+1} \geq 0$, $D_M^{k+1} \geq 0$, $D_C^{k+1} \geq 0$, $D_F^{k+1} \geq 0$, $J_M^{k+1} \geq 0$, $J_C^{k+1} \geq 0$, and $J_F^{k+1} \geq 0$, when the discrete variables from the preceding iteration are non-negative, requires proof of k positive invariance. The equations of (24) added together produce

$$\begin{aligned}
(1+\varphi\kappa)G^{k+1} &\leq \varphi\tau + G^k,\\
G^{k+1} &\leq \frac{\tau}{\kappa}, \quad if \quad G^k \leq \frac{\tau}{\kappa}.
\end{aligned} \tag{27}$$

Here, $G^k = M^k+C^k+F^k+D_M^k+D_C^k+D_F^k+J_M^k+J_C^k+J_F^k$ denotes the total population at the (k)-th time step, $\tau = \pi_1+\pi_2+\pi_3$ represents the total recruitment term, and $\kappa = \nu$ denotes the common natural removal rate. The a priori connections for J_F^{k+1} and J_C^{k+1} result from the fact that J_F^{k+1} and C^{k+1} are $\geq G^{k+1}$ and have a radial symmetry. This completes the proof. □

5.2. Results of suggested scheme

The Nonstandard Finite Difference (NSFD) method was used in numerical simulations to examine the dynamics of the proposed smoking-induced asthma and cardiovascular model. Realistic interaction rates between smoking behavior and the emergence of asthma and heart-related problems are reflected in the parameter set chosen for the simulations. The system under development makes use of the following parameter values: $\pi_1 = 600$; $\pi_2 = 400$; $\pi_3 = 160$; $\beta_1 = 0.575$; $\beta_2 = 0.683$; $\beta_3 = 0.77$; $\nu = 0.0002$; $\delta = 0.514$; $j_1 = 0.04$; $j_2 = 0.024$; $j_3 = 0.027$; $l_1 = 0.044$; $l_2 = 0.018$; $l_3 = 0.048$. The population classifications that are included in the developed system are the ex-smoker class, the active-smoker class, and the

non-smoker class. Six subgroups comprise the population with smoking-related asthma and cardiovascular diseases: D_M, D_C, D_F, J_M, J_C, and J_F. The NSFD scheme with a length of $\phi = 0.1$ has been used to determine the convergence behavior of both the baseline smoking equilibrium (BSE) and positive equilibrium (PE). Additionally, the convergence results are shown for $\phi(h) = h + O(h^2)$, confirming the stability and correctness of the suggested numerical technique.

Figures 14, 15a, and 15b show how well the approach controls asthma and cardiovascular disorders caused by smoking. The convergence of the proposed model toward the baseline smoking equilibrium is illustrated in Figure 14. The non-smoker population approaches its steady-state level, whereas the smoker, ex-smoker, and smoking-induced disease-prevalence sub-populations gradually decrease to zero. This behavior indicates that, in the absence of sustained smoking-induced disease progression, the system converges to the baseline smoking equilibrium, where the smoking-status populations remain at steady state and no asthma or cardiovascular disease prevalence persists.

Figure 15a illustrates the convergence of the proposed model toward the positive equilibrium, where both the smoking-status populations and the smoking-induced disease-prevalence sub-populations attain positive steady-state values. The numerical trajectories show that continuous smoking exposure sustains non-zero levels of asthma and cardiovascular disease prevalence. Figure 15b presents the corresponding dynamics under larger initial population sizes. Although the initial conditions differ substantially, all state variables converge to the same positive equilibrium. This demonstrates that the proposed NSFD scheme preserves the qualitative behavior of the continuous model and produces consistent solutions irrespective of the selected biologically feasible initial populations. Overall, the numerical results confirm that the proposed NSFD scheme preserves positivity, boundedness, and the qualitative dynamical behavior of the continuous model. Consequently, the numerical solutions remain biologically meaningful throughout the simulation interval and accurately describe the long-term evolution of smoking populations together with smoking-induced asthma and cardiovascular disease prevalence.

The proposed NSFD scheme demonstrates clear advantages over the classical Euler and standard finite difference methods. Unlike conventional schemes, which may fail to preserve positivity or produce nonphysical oscillations in nonlinear population models, the proposed NSFD formulation guarantees the positivity and boundedness of all state variables for biologically feasible initial conditions. Furthermore, it preserves the qualitative dynamics of the continuous model, including convergence toward both the baseline smoking equilibrium and the positive equilibrium, without introducing numerical artifacts. Owing to the use of a nonstandard denominator function, the scheme also remains stable for relatively larger time-step sizes, thereby improving computational efficiency.

6. Optimal control strategy for the suggested model

This section's goal is to examine how the smoking model applies to the optimum control strategy. Preventive control factors like social media awareness $\hbar_1$ and a therapeutic control measure used by victims to reduce the presence of smoking-related health complications in their bodies $\hbar_2$ are potential participants in reducing illness prevalence in peers. As an action variable that can be changed to get the desired outcome, the control variable establishes the best values for choice variables. Determining the most effective strategy requires choosing the optimal value for the control variables. We apply the ideas of optimum control theory [22, 26, 27] to create a control methodology. The differential construction of the model supplied equation (10), which is as follows, now includes the control variable:

$$\begin{aligned}
\frac{dM}{dt} &= \pi_1 - (1-\hbar_1)\beta_1 MC - \nu M,\\
\frac{dC}{dt} &= \pi_2 - (1-\hbar_1)\beta_3 C - \delta C - \nu C,\\
\frac{dF}{dt} &= \pi_3 + \delta C - (1-\hbar_1)\beta_2 FC - \nu F,\\
\frac{dD_M}{dt} &= (1-\hbar_1) j_1\beta_1 MC - (\kappa_1\hbar_2 + \nu)D_M,\\
\frac{dD_C}{dt} &= (1-\hbar_1) j_3\beta_3 C - (\kappa_1\hbar_2 + \nu)D_C,\\
\frac{dD_F}{dt} &= (1-\hbar_1) j_2\beta_2 FC - (\kappa_1\hbar_2 + \nu)D_F,\\
\frac{dJ_M}{dt} &= (1-\hbar_1) l_1\beta_1 MC - (\kappa_1\hbar_2 + \nu)J_M,\\
\frac{dJ_C}{dt} &= (1-\hbar_1) l_3\beta_3 C - (\kappa_1\hbar_2 + \nu)J_C,\\
\frac{dJ_F}{dt} &= (1-\hbar_1) l_2\beta_2 FC - (\kappa_1\hbar_2 + \nu)J_F,
\end{aligned} \tag{28}$$

under certain initial circumstances. As a result, we examine an optimum control issue where the objective function in Ref. [44] has the following definition and expression:

$$\begin{aligned}
K(\hbar_1(t), \hbar_2(t)) = \int_0^t \{&Y_1 D_M(t) + Y_2 D_C(t) + Y_3 D_F(t) + Y_4 J_M(t)\\
&+ Y_5 J_C(t) + Y_6 J_F(t) + \frac{1}{2}X_1\hbar_1^2(t) + \frac{1}{2}X_2\hbar_2^2(t)\}dt.
\end{aligned} \tag{29}$$

In this case, $Y_1, Y_2, Y_3, Y_4, Y_5, and Y_6$ represent the weight constants for each class, and $X_k \geq 0$, $k = 1, 2$ represents the cost of control. For control pairs, the objective function is minimized as follows:

$$K(\hbar_1^*, \hbar_2^*) = min\{K(\hbar_1(t), \hbar_2(t)), \hbar_1(t), \hbar_2(t) \in \mathfrak{Z}\}. \tag{30}$$

The control system (28) affects the optimization process, and the suitably defined control set $\mathfrak{Z}$ is:

$$\begin{aligned}
\mathfrak{Z} = \{(\hbar_1, \hbar_2) \setminus \hbar_k(t) \text{ is Lebesgue measurable on } [0,1],\\
0 \leq \hbar_k(t) \leq 1,\ k = 1, 2\}.
\end{aligned} \tag{31}$$

Pontryagin's Maximum Principle is also used to identify the optimal control strategies for dynamical systems. It offers necessary circumstances for arriving at the optimal solution

by directing the selection of controls for an objective function K. This direction is obtained by analyzing the behavior of the Hamiltonian function T at each location in the state variable.

Theorem 6.1. There is a $\hbar^*(t) = (\hbar_1^*(t), \hbar_2^*(t) \in \Im)$ for the optimal control problem (28), such that

$$min_{(\hbar_1(t),\hbar_2(t)\in\Im)} K(\hbar_1(t), \hbar_2(t)) = K(\hbar_1(t), \hbar_2(t)).$$

Proof. The efficacy control scheme in Ref. [21, 25] is examined in a number of ways, and both the control and state variables are determined to have non-negative values. The necessary stability of the control system is defined by the convexity and proximity of the control variables. Furthermore, the convex shape of the integrand contains an objective function written as $Y_1D_M(t) + Y_2D_C(t) + Y_3D_F(t) + Y_4J_M(t) + Y_5J_C(t) + Y_6J_F(t) + \frac{1}{2}X_1\hbar_1^2(t) + \frac{1}{2}X_2\hbar_2^2(t)$, which attests to the proof, where $X_k \geq 0$, $k = 1, 2$ represents the cost of control and $Y_k, k = 1, 2, 3, 4, 5, 6$ represents the weight constants associated with each class. To address our proposed problem, we apply the Pontryagin maximum principle [45–47] once more. The following is an explicit definition of the Hamiltonian function:

$$\begin{aligned} T = {} & L(M, C, F, D_M, D_C, D_F, J_M, J_C, J_F, \hbar_1, \hbar_2) + \xi_1 \frac{dM}{dt} \\ & + \xi_2 \frac{dC}{dt} + \xi_3 \frac{dF}{dt} + \xi_4 \frac{dD_M}{dt} + \xi_5 \frac{dD_C}{dt} + \xi_6 \frac{dD_F}{dt} \\ & + \xi_7 \frac{dJ_M}{dt} + \xi_8 \frac{dJ_C}{dt} + \xi_9 \frac{dJ_F}{dt}. \end{aligned} \tag{32}$$

The existence of non-trivial vectors, denoted as $\xi(t) = (\xi_1, \xi_2, \xi_3, \xi_4, \xi_5, \xi_6, \xi_7, \xi_8, \xi_9)$, becomes evident while evaluating $(V(t), \hbar(t))$ as the optimal approach for the initiated control issue.

$$\begin{aligned} \frac{dV(t)}{dt} &= \frac{\partial T(t, V(t), \hbar(t), \xi(t))}{\partial \xi_k}, \quad k = 1, 2, \ldots, 9. \\ 0 &= \frac{\partial T(t, V(t), \hbar(t), \xi(t))}{\partial \hbar_i}, \quad i = 1, 2. \\ \xi_k^{'} &= \frac{\partial T(t, V(t), \hbar(t), \xi(t))}{\partial V(t)}, \quad k = 1, 2, \ldots, 9. \end{aligned} \tag{33}$$

The transversal condition is as follows: $\xi_k(t) = 0$, $k = 1, \ldots, 9$. To obtain the results, the essential condition is also applied to the Hamiltonian function. □

6.1. Existence of the optimal control problem

Pontryagin's maximum principle is used to establish the necessary conditions for an optimal result by taking into account the initial time $t = 0$. We maintain a Lebesgue measurable and limited control [25, 48] in order to accomplish these goals. The upward boundedness of the system's solution is guaranteed, and this control is dependent on initial conditions. A thorough examination of the Lagrangian and Hamiltonian is used to solve the optimal control problem. The optimal control problem is formulated using the Lagrangian framework, and the relevant equation is expressed as follows: the control set $\Im$ for the control strategy is defined using the dependent constructed system (28).

$$\begin{aligned} L\{M, C, F, D_M, D_C, D_F, J_M, J_C, J_F, \hbar_1, \hbar_2\} = {} & Y_1D_M(t) \\ & + Y_2D_C(t) + Y_3D_F(t) + Y_4J_M(t) + Y_5J_C(t) + Y_6J_F(t) \\ & + \frac{1}{2}X_1\hbar_1^2(t) + \frac{1}{2}X_2\hbar_2^2(t). \end{aligned} \tag{34}$$

The Hamiltonian function T for the model can be found in (32). After entering the Lagrangian equation and the values of each compartment, T may be expressed using equation (32).

$$\begin{cases} T(V(t), \xi(t), \hbar(t)) = Y_1D_M(t) + Y_2D_C(t) + Y_3D_F(t) + Y_4J_M(t) \\ + Y_5J_C(t) + Y_6J_F(t) + \frac{1}{2}X_1\hbar_1^2(t) + \frac{1}{2}X_2\hbar_2^2(t) \\ + \xi_1 [\pi_1 - (1 - \hbar_1)\beta_1 MC - \nu M] \\ + \xi_2 [\pi_2 - (1 - \hbar_1)\beta_3 C - \delta C - \nu C] \\ + \xi_3 [\pi_3 + \delta C - (1 - \hbar_1)\beta_2 FC - \nu F] \\ + \xi_4 [(1 - \hbar_1) j_1\beta_1 MC - (\kappa_1\hbar_2 + \nu)D_M] \\ + \xi_5 [(1 - \hbar_1) j_3\beta_3 C - (\kappa_1\hbar_2 + \nu)D_C] \\ + \xi_6 [(1 - \hbar_1) j_2\beta_2 FC - (\kappa_1\hbar_2 + \nu)D_F] \\ + \xi_7 [(1 - \hbar_1) l_1\beta_1 MC - (\kappa_1\hbar_2 + \nu)J_M] \\ + \xi_8 [(1 - \hbar_1) l_3\beta_3 C - (\kappa_1\hbar_2 + \nu)J_C] \\ + \xi_9 [(1 - \hbar_1) l_2\beta_2 FC - (\kappa_1\hbar_2 + \nu)J_F]. \end{cases} \tag{35}$$

$V(t) = (M(t), C(t), F(t), D_M(t), D_C(t), D_F(t), J_M(t), J_C(t), J_F(t))$ represents a vector of state variables, and $\xi_k(t)$ for $k = 1, 2, \ldots, 9$ represents the adjoint variables that correspond to the state equations of the system (28). We also develop the basic optimality criterion for the equations (28) and (29);

$$\begin{aligned} \frac{dV(t)}{dt} &= \frac{\partial T(t, V(t), \hbar(t), \xi(t))}{\partial \xi_k}, \quad k = 1, 2, \ldots, 9. \\ 0 &= \frac{\partial T(t, V(t), \hbar(t), \xi(t))}{\partial \hbar_i}, \quad i = 1, 2. \\ \xi_k^{'} &= \frac{\partial T(t, V(t), \hbar(t), \xi(t))}{\partial V(t)}, \quad k = 1, 2, \ldots, 9. \end{aligned} \tag{36}$$

The transversality condition can be expressed as $\xi_k(t) = 0$ for $k = 1, 2, \ldots, 9$. The resulting system can be described as follows: $\xi_1, \xi_2, \xi_3, \xi_4, \xi_5, \xi_6, \xi_7, \xi_8$, and ξ_9 in addition to the optimal control variables $\hbar_1$ and $\hbar_2$.

$$\begin{aligned} \dot{\xi}_1 &= \xi_1 [(1 - \hbar_1)\beta_1 C + \nu] - \xi_4 [(1 - \hbar_1) j_1\beta_1 C] - \\ & \xi_7 [(1 - \hbar_1) l_1\beta_1 C], \\ \dot{\xi}_2 &= \xi_1 [(1 - \hbar_1)\beta_1 M] + \xi_2 [(1 - \hbar_1)\beta_3 + \delta + \nu] \\ & - \xi_3 [\delta - (1 - \hbar_1)\beta_2 F] - \xi_4 [(1 - \hbar_1) j_1\beta_1 M] \\ & - \xi_5 [(1 - \hbar_1) j_3\beta_3] - \xi_6 [(1 - \hbar_1) j_2\beta_2 F] - \xi_7 [(1 - \hbar_1) l_1\beta_1 M] \\ & - \xi_8 [(1 - \hbar_1) l_3\beta_3] - \xi_9 [(1 - \hbar_1) l_2\beta_2 F], \\ \dot{\xi}_3 &= \xi_3 [(1 - \hbar_1)\beta_2 C + \nu] - \xi_6 [(1 - \hbar_1) j_2\beta_2 C] \\ & - \xi_9 [(1 - \hbar_1) l_2\beta_2 C], \\ \dot{\xi}_4 &= Y_1 - \xi_4(\kappa_1\hbar_2 + \nu), \\ \dot{\xi}_5 &= Y_2 - \xi_5(\kappa_1\hbar_2 + \nu), \\ \dot{\xi}_6 &= Y_3 - \xi_6(\kappa_1\hbar_2 + \nu), \end{aligned}$$

$$\begin{aligned}
\dot{\xi}_7 &= Y_4 - \xi_7(\kappa_1\hbar_2 + \nu),\\
\dot{\xi}_8 &= Y_5 - \xi_8(\kappa_1\hbar_2 + \nu),\\
\dot{\xi}_9 &= Y_6 - \xi_9(\kappa_1\hbar_2 + \nu),\\
\hbar_1 &= \frac{(\xi_1 - \xi_4 j_1 - \xi_7 l_1)\beta_1 MC + (\xi_2 - \xi_5 j_3 - \xi_8 l_3)\beta_3 C}{-X_1},\\
&+ \frac{(\xi_3 - \xi_6 j_2 - \xi_9 l_2)\beta_2 FC}{-X_1}\\
\hbar_2 &= \frac{\kappa_1(\xi_4 D_M + \xi_5 D_C + \xi_6 D_F + \xi_7 J_M + \xi_8 J_C + \xi_9 J_F)}{X_2}. \qquad (37)
\end{aligned}$$

Theorem 6.2. Given the optimal controls $\hbar_1^*$ and $\hbar_2^*$ and the solution $M^*(t)$, $C^*(t)$, $F^*(t)$, $D_M^*(t)$, $D_C^*(t)$, $D_F^*(t)$, $J_M^*(t)$, $J_C^*(t)$, $J_F^*(t)$ of the corresponding state structure (28), the nearby variables $\xi_k(t)$, $k = 1, 2, \ldots, 9$ exist such that:

$$\begin{aligned}
\dot{\xi}_1 &= \xi_1\left[(1-\hbar_1)\beta_1 C + \nu\right] - \xi_4\left[(1-\hbar_1)j_1\beta_1 C\right]\\
&- \xi_7\left[(1-\hbar_1)l_1\beta_1 C\right],\\
\dot{\xi}_2 &= \xi_1\left[(1-\hbar_1)\beta_1 M\right] + \xi_2\left[(1-\hbar_1)\beta_3 + \delta + \nu\right]\\
&- \xi_3\left[\delta - (1-\hbar_1)\beta_2 F\right]\\
&- \xi_4\left[(1-\hbar_1)j_1\beta_1 M\right] - \xi_5\left[(1-\hbar_1)j_3\beta_3\right]\\
&- \xi_6\left[(1-\hbar_1)j_2\beta_2 F\right]\\
&- \xi_7\left[(1-\hbar_1)l_1\beta_1 M\right] - \xi_8\left[(1-\hbar_1)l_3\beta_3\right] - \xi_9\left[(1-\hbar_1)l_2\beta_2 F\right],\\
\dot{\xi}_3 &= \xi_3\left[(1-\hbar_1)\beta_2 C + \nu\right] - \xi_6\left[(1-\hbar_1)j_2\beta_2 C\right]\\
&- \xi_9\left[(1-\hbar_1)l_2\beta_2 C\right],\\
\dot{\xi}_4 &= Y_1 - \xi_4(\kappa_1\hbar_2 + \nu),\\
\dot{\xi}_5 &= Y_2 - \xi_5(\kappa_1\hbar_2 + \nu),\\
\dot{\xi}_6 &= Y_3 - \xi_6(\kappa_1\hbar_2 + \nu),\\
\dot{\xi}_7 &= Y_4 - \xi_7(\kappa_1\hbar_2 + \nu),\\
\dot{\xi}_8 &= Y_5 - \xi_8(\kappa_1\hbar_2 + \nu), \qquad (38)\\
\dot{\xi}_9 &= Y_6 - \xi_9(\kappa_1\hbar_2 + \nu), \qquad (39)
\end{aligned}$$

by using $\xi_k(t)$, $k = 1, 2, \ldots, 9$, the transversality condition.

Proof. Assume for the moment that the state variables $M(t) = M^*(t)$, $C(t) = C^*(t)$, $F(t) = F^*(t)$, $D_M(t) = D_M^*(t)$, $D_C(t) = D_C^*(t)$, $D_F(t) = D_F^*(t)$, $J_M(t) = J_M^*(t)$, $J_C(t) = J_C^*(t)$, and $J_F(t) = J_F^*(t)$. The state variables $M(t)$, $C(t)$, $F(t)$, $D_M(t)$, $D_C(t)$, $D_F(t)$, $J_M(t)$, $J_C(t)$, and $J_F(t)$ are also used to describe the Hamiltonian. Subject to the transversality condition, the enhanced adjoint system is now displayed as follows:

$$\begin{aligned}
\dot{\xi}_1 &= \xi_1\left[(1-\hbar_1)\beta_1 C + \nu\right] - \xi_4\left[(1-\hbar_1)j_1\beta_1 C\right]\\
&- \xi_7\left[(1-\hbar_1)l_1\beta_1 C\right],\\
\dot{\xi}_2 &= \xi_1\left[(1-\hbar_1)\beta_1 M\right] + \xi_2\left[(1-\hbar_1)\beta_3 + \delta + \nu\right]\\
&- \xi_3\left[\delta - (1-\hbar_1)\beta_2 F\right]\\
&- \xi_4\left[(1-\hbar_1)j_1\beta_1 M\right] - \xi_5\left[(1-\hbar_1)j_3\beta_3\right]\\
&- \xi_6\left[(1-\hbar_1)j_2\beta_2 F\right]\\
&- \xi_7\left[(1-\hbar_1)l_1\beta_1 M\right] - \xi_8\left[(1-\hbar_1)l_3\beta_3\right] - \xi_9\left[(1-\hbar_1)l_2\beta_2 F\right],\\
\dot{\xi}_3 &= \xi_3\left[(1-\hbar_1)\beta_2 C + \nu\right] - \xi_6\left[(1-\hbar_1)j_2\beta_2 C\right]\\
&- \xi_9\left[(1-\hbar_1)l_2\beta_2 C\right],\\
\dot{\xi}_4 &= Y_1 - \xi_4(\kappa_1\hbar_2 + \nu),\ \dot{\xi}_5 = Y_2 - \xi_5(\kappa_1\hbar_2 + \nu),\\
\dot{\xi}_6 &= Y_3 - \xi_6(\kappa_1\hbar_2 + \nu),\ \dot{\xi}_7 = Y_4 - \xi_7(\kappa_1\hbar_2 + \nu),\\
\dot{\xi}_8 &= Y_5 - \xi_8(\kappa_1\hbar_2 + \nu),\ \dot{\xi}_9 = Y_6 - \xi_9(\kappa_1\hbar_2 + \nu), \qquad (40)
\end{aligned}$$

□

Theorem 6.3. For the area $\mathfrak{Z}$, the optimal control pair $(\hbar_1^*(t), \hbar_2^*(t))$ is as follows:

$$\begin{aligned}
\hbar_1^*(t) &= \max\left\{0, \min\left\{1, \frac{1}{-X_1}\Big[(\xi_1 - \xi_4 j_1 - \xi_7 l_1)\beta_1 MC\right.\right.\\
&\left.\left. + (\xi_2 - \xi_5 j_3 - \xi_8 l_3)\beta_3 C + (\xi_3 - \xi_6 j_2 - \xi_9 l_2)\beta_2 FC\Big]\right\}\right\},\\
\hbar_2^*(t) &= \max\left\{0, \min\left\{1, \frac{\kappa_1}{X_2}\Big(\xi_4 D_M + \xi_5 D_C + \xi_6 D_F + \xi_7 J_M\right.\right.\\
&\left.\left. + \xi_8 J_C + \xi_9 J_F\Big)\right\}\right\}. \qquad (41)
\end{aligned}$$

Proof. When perfect circumstances were met, the following outcomes were obtained:

$$\begin{aligned}
\frac{\partial T}{\partial \hbar_1} &= X_1\hbar_1 + (\xi_1 - \xi_4 j_1 - \xi_7 l_1)\beta_1 MC + (\xi_2 - \xi_5 j_3 - \xi_8 l_3)\beta_3 C\\
&+ (\xi_3 - \xi_6 j_2 - \xi_9 l_2)\beta_2 FC,\\
\frac{\partial T}{\partial \hbar_2} &= X_2\hbar_2 - \kappa_1(\xi_4 D_M + \xi_5 D_C + \xi_6 D_F + \xi_7 J_M + \xi_8 J_C + \xi_9 J_F), \qquad (42)
\end{aligned}$$

The control variable is:

$$\begin{aligned}
\hbar_1^*(t) &= \frac{1}{-X_1}\Big[(\xi_1 - \xi_4 j_1 - \xi_7 l_1)\beta_1 MC + (\xi_2 - \xi_5 j_3 - \xi_8 l_3)\beta_3 C\\
&+ (\xi_3 - \xi_6 j_2 - \xi_9 l_2)\beta_2 FC\Big],\\
\hbar_2^*(t) &= \frac{\kappa_1(\xi_4 D_M + \xi_5 D_C + \xi_6 D_F + \xi_7 J_M + \xi_8 J_C + \xi_9 J_F)}{X_2}, \qquad (43)
\end{aligned}$$

It is evident that the state of control space is still covered by the following expression:

$$\hbar_1^*(t) = \begin{cases}
0, \text{ if } \frac{1}{-X_1}\Big[(\xi_1 - \xi_4 j_1 - \xi_7 l_1)\beta_1 MC\\
+ (\xi_2 - \xi_5 j_3 - \xi_8 l_3)\beta_3 C\\
+ (\xi_3 - \xi_6 j_2 - \xi_9 l_2)\beta_2 FC\Big] \le 0,\\
\frac{1}{-X_1}\Big[(\xi_1 - \xi_4 j_1 - \xi_7 l_1)\beta_1 MC + (\xi_2 - \xi_5 j_3 - \xi_8 l_3)\beta_3 C\\
+ (\xi_3 - \xi_6 j_2 - \xi_9 l_2)\beta_2 FC\Big], \text{if } 0 < \frac{1}{-X_1}\Big[(\xi_1 - \xi_4 j_1 - \xi_7 l_1)\\
\times\beta_1 MC + (\xi_2 - \xi_5 j_3 - \xi_8 l_3)\beta_3 C\\
+ (\xi_3 - \xi_6 j_2 - \xi_9 l_2)\beta_2 FC\Big] < 1,\\
1, \text{ if } \frac{1}{-X_1}\Big[(\xi_1 - \xi_4 j_1 - \xi_7 l_1)\beta_1 MC + (\xi_2 - \xi_5 j_3 - \xi_8 l_3)\\
\times\beta_3 C\\
+ (\xi_3 - \xi_6 j_2 - \xi_9 l_2)\beta_2 FC\Big] \ge 1.
\end{cases}$$

$$\hbar_2^*(t) = \begin{cases} 0, \text{ if } \dfrac{\kappa_1(\xi_4 D_M + \xi_5 D_C + \xi_6 D_F + \xi_7 J_M + \xi_8 J_C + \xi_9 J_F)}{X_2} \le 0, \\ \dfrac{\kappa_1(\xi_4 D_M + \xi_5 D_C + \xi_6 D_F + \xi_7 J_M + \xi_8 J_C + \xi_9 J_F)}{X_2}, \\ \text{if } 0 < \dfrac{\kappa_1(\xi_4 D_M + \xi_5 D_C + \xi_6 D_F + \xi_7 J_M + \xi_8 J_C + \xi_9 J_F)}{X_2} < 1, \\ 1, \text{ if } \dfrac{\kappa_1(\xi_4 D_M + \xi_5 D_C + \xi_6 D_F + \xi_7 J_M + \xi_8 J_C + \xi_9 J_F)}{X_2} \ge 1. \end{cases}$$

Simplified, the variables under control are

$$\begin{aligned} \hbar_1^*(t) &= \max\left\{0, \min\left\{1, \frac{1}{-X_1}\Big[(\xi_1 - \xi_4 j_1 - \xi_7 l_1)\beta_1 MC \right.\right. \\ &\quad \left.\left. + (\xi_2 - \xi_5 j_3 - \xi_8 l_3)\beta_3 C + (\xi_3 - \xi_6 j_2 - \xi_9 l_2)\beta_2 FC\Big]\right\}\right\}, \\ \hbar_2^*(t) &= \max\left\{0, \min\left\{1, \frac{\kappa_1}{X_2}\Big(\xi_4 D_M + \xi_5 D_C + \xi_6 D_F + \xi_7 J_M \right.\right. \\ &\quad \left.\left. + \xi_8 J_C + \xi_9 J_F\Big)\right\}\right\}. \end{aligned} \tag{44}$$

The ideal system is now provided as:

$$\begin{aligned} \frac{dM^*}{dt} &= \pi_1 - (1 - \max\left\{0, \min\left\{1, \frac{1}{-X_1}\Big[(\xi_1 - \xi_4 j_1 - \xi_7 l_1)\beta_1 MC \right.\right. \\ &\quad \left.\left. + (\xi_2 - \xi_5 j_3 - \xi_8 l_3)\beta_3 C + (\xi_3 - \xi_6 j_2 - \xi_9 l_2)\beta_2 FC\Big]\right\}\right\})(\beta_1 C - \nu)M, \\ \frac{dC^*}{dt} &= \pi_2 - (1 - \max\left\{0, \min\left\{1, \frac{1}{-X_1}\Big[(\xi_1 - \xi_4 j_1 - \xi_7 l_1)\beta_1 MC \right.\right. \\ &\quad \left.\left. + (\xi_2 - \xi_5 j_3 - \xi_8 l_3)\beta_3 C + (\xi_3 - \xi_6 j_2 - \xi_9 l_2)\beta_2 FC\Big]\right\}\right\})(\beta_3 - \delta - \nu)C, \\ \frac{dF^*}{dt} &= \pi_3 + \delta C - (1 - \max\left\{0, \min\left\{1, \frac{1}{-X_1}\Big[(\xi_1 - \xi_4 j_1 - \xi_7 l_1)\beta_1 MC \right.\right. \\ &\quad \left.\left. + (\xi_2 - \xi_5 j_3 - \xi_8 l_3)\beta_3 C + (\xi_3 - \xi_6 j_2 - \xi_9 l_2)\beta_2 FC\Big]\right\}\right\})(\beta_2 C - \nu)F, \\ \frac{dD_M^*}{dt} &= (1 - \max\left\{0, \min\left\{1, \frac{1}{-X_1}\Big[(\xi_1 - \xi_4 j_1 - \xi_7 l_1)\beta_1 MC \right.\right. \\ &\quad \left.\left. + (\xi_2 - \xi_5 j_3 - \xi_8 l_3)\beta_3 C + (\xi_3 - \xi_6 j_2 - \xi_9 l_2)\beta_2 FC\Big]\right\}\right\})j_1\beta_1 MC - \nu D_M \\ &\quad - \kappa_1(\max\left\{0, \min\left\{1, \frac{\kappa_1(\xi_4 D_M + \xi_5 D_C + \xi_6 D_F + \xi_7 J_M + \xi_8 J_C + \xi_9 J_F)}{X_2}\right\}\right\})D_M, \\ \frac{dD_C^*}{dt} &= (1 - \max\left\{0, \min\left\{1, \frac{1}{-X_1}\Big[(\xi_1 - \xi_4 j_1 - \xi_7 l_1)\beta_1 MC \right.\right. \\ &\quad \left.\left. + (\xi_2 - \xi_5 j_3 - \xi_8 l_3)\beta_3 C + (\xi_3 - \xi_6 j_2 - \xi_9 l_2)\beta_2 FC\Big]\right\}\right\})j_3\beta_3 C - \nu D_C \\ &\quad - \kappa_1(\max\left\{0, \min\left\{1, \frac{\kappa_1(\xi_4 D_M + \xi_5 D_C + \xi_6 D_F + \xi_7 J_M + \xi_8 J_C + \xi_9 J_F)}{X_2}\right\}\right\})D_C, \\ \frac{dD_F^*}{dt} &= (1 - \max\left\{0, \min\left\{1, \frac{1}{-X_1}\Big[(\xi_1 - \xi_4 j_1 - \xi_7 l_1)\beta_1 MC \right.\right. \\ &\quad \left.\left. + (\xi_2 - \xi_5 j_3 - \xi_8 l_3)\beta_3 C + (\xi_3 - \xi_6 j_2 - \xi_9 l_2)\beta_2 FC\Big]\right\}\right\})j_2\beta_2 FC - \nu D_F \\ &\quad - \kappa_1(\max\left\{0, \min\left\{1, \frac{\kappa_1(\xi_4 D_M + \xi_5 D_C + \xi_6 D_F + \xi_7 J_M + \xi_8 J_C + \xi_9 J_F)}{X_2}\right\}\right\})D_F, \end{aligned}$$

$$\begin{aligned} \frac{dJ_M^*}{dt} &= (1 - \max\left\{0, \min\left\{1, \frac{1}{-X_1}\Big[(\xi_1 - \xi_4 j_1 - \xi_7 l_1)\beta_1 MC \right.\right. \\ &\quad \left.\left. + (\xi_2 - \xi_5 j_3 - \xi_8 l_3)\beta_3 C + (\xi_3 - \xi_6 j_2 - \xi_9 l_2)\beta_2 FC\Big]\right\}\right\})l_1\beta_1 MC - \nu J_M \\ &\quad - \kappa_1(\max\left\{0, \min\left\{1, \frac{\kappa_1(\xi_4 D_M + \xi_5 D_C + \xi_6 D_F + \xi_7 J_M + \xi_8 J_C + \xi_9 J_F)}{X_2}\right\}\right\})J_M, \\ \frac{dJ_C^*}{dt} &= (1 - \max\left\{0, \min\left\{1, \frac{1}{-X_1}\Big[(\xi_1 - \xi_4 j_1 - \xi_7 l_1)\beta_1 MC \right.\right. \\ &\quad \left.\left. + (\xi_2 - \xi_5 j_3 - \xi_8 l_3)\beta_3 C + (\xi_3 - \xi_6 j_2 - \xi_9 l_2)\beta_2 FC\Big]\right\}\right\})l_3\beta_3 C - \nu J_C \\ &\quad - \kappa_1(\max\left\{0, \min\left\{1, \frac{\kappa_1(\xi_4 D_M + \xi_5 D_C + \xi_6 D_F + \xi_7 J_M + \xi_8 J_C + \xi_9 J_F)}{X_2}\right\}\right\})J_C, \\ \frac{dJ_F^*}{dt} &= (1 - \max\left\{0, \min\left\{1, \frac{1}{-X_1}\Big[(\xi_1 - \xi_4 j_1 - \xi_7 l_1)\beta_1 MC \right.\right. \\ &\quad \left.\left. + (\xi_2 - \xi_5 j_3 - \xi_8 l_3)\beta_3 C + (\xi_3 - \xi_6 j_2 - \xi_9 l_2)\beta_2 FC\Big]\right\}\right\})l_2\beta_2 FC - \nu J_F \\ &\quad - \kappa_1(\max\left\{0, \min\left\{1, \frac{\kappa_1(\xi_4 D_M + \xi_5 D_C + \xi_6 D_F + \xi_7 J_M + \xi_8 J_C + \xi_9 J_F)}{X_2}\right\}\right\})J_F. \end{aligned} \tag{45}$$

In optimization, an adjacent variable is used in conjunction with the ideal system and initial conditions to identify the variables of state and control. It is clear that the second-order derivative of the desired function is positive with respect to the control variables. As a result, the final Hamiltonian's formal documentation is as follows:

$$\begin{aligned} T^* &= Y_1 D_M^*(t) + Y_2 D_C^*(t) + Y_3 D_F^*(t) + Y_4 J_M^*(t) + Y_5 J_C^*(t) \\ &\quad + Y_6 J_F^*(t) + \frac{1}{2} X_1 \hbar_1^2(t) + \frac{1}{2} X_2 \hbar_2^2(t) \\ &\quad + \sum_{k=1}^{9} \xi_k h_k(M^*, C^*, F^*, D_M^*, D_C^*, D_F^*, J_M^*, J_C^*, J_F^*). \end{aligned}$$

□

6.2. Discussion and numerical simulation

To validate the analytical outcomes of the smoking model, we performed numerical simulations using the Nonstandard Finite Difference Scheme. The best control measures, such as treatment methods $\hbar_2$ and a social media awareness campaign $\hbar_1$, were used to solve the system in two alternative ways. At steps $k = 0$ and $k = t$, the adjoint variables ξ_i for $i = 1, 2, ..., 9$ are then solved backward, while the state variables $M, C, F, D_M, D_C, D_F, J_M, J_C$, and J_F are solved forward iteratively. In this study, we focused on the system's description of smoking and employed numerical simulations to demonstrate our theoretical findings (28). We used parameter values depicted in Table 2. The numerical data used in this study are obtained from two sources: (i) previously published epidemiological models on smoking dynamics, and (ii) a school-based survey conducted in the Turkish Republic of Northern Cyprus (TRNC) during 2020, from which smoking initiation rates, smoking prevalence, and transition-related behavioral parameters were derived. Since the primary objective of this study is to investigate the qualitative dynamics and optimal control behavior of the proposed model rather than statistical forecasting, no formal parameter calibration procedure was performed. Parameters for which no directly measured clinical estimates were available were selected within biologically reasonable

ranges to ensure realistic numerical simulations. All rate parameters are expressed on a yearly basis (year^{-1}), while the population compartments represent the number of individuals. These data are used to initialize the system and validate the qualitative behavior of the model. The initial values were chosen as $M(0) = 60, C(0) = 30, F(0) = 45, D_M(0) = 50, D_C(0) = 22, D_F(0) = 32, J_M(0) = 45, J_C(0) = 42, J_F(0) = 31$. Moreover, the weight constant is set to be $X_1 = 0.5 = X_2$.

Figure 16 illustrates the temporal dynamics of the non-smoker population $M(t)$ and the active-smoker population $C(t)$ under controlled and uncontrolled scenarios. In Figure 16a, the non-smoker class experiences a sharp decline during the initial period in both cases. However, when control measures are implemented, the population subsequently recovers and remains above the uncontrolled trajectory. Towards the end of the time interval, the controlled solution exhibits a noticeable increase, demonstrating the cumulative effectiveness of the control strategy. Figure 16b presents the behaviour of active-smokers $C(t)$. The number of active smokers decreases continuously over time in both cases, reflecting a reduction in smoking prevalence. The controlled trajectory declines more rapidly after the early stages and remains lower than the uncontrolled case for a substantial portion of the simulation period. This behaviour suggests that the implemented controls are successful in limiting smoking initiation and encouraging smoking cessation. These findings indicate that sustained awareness campaigns together with appropriate treatment strategies can effectively shift individuals away from smoking behaviour. As the number of active smokers decreases, the non-smoker population gradually recovers, reducing the long-term exposure of the community to smoking-related health risks. This highlights the importance of combining preventive education with clinical intervention to improve overall public health.

Figure 17 depicts the evolution of ex-smokers $F(t)$ and non-smokers suffering from asthma $D_M(t)$. In Figure 17a, the ex-smoker population decreases sharply at the beginning of the simulation, followed by a gradual stabilization. Under the controlled scenario, the trajectory remains slightly above the uncontrolled solution during the intermediate period. A pronounced increase near the end of the simulation further confirms the positive influence of the control measures on maintaining individuals in the ex-smoker class. Figure 17b shows the dynamics of $D_M(t)$. The uncontrolled solution exhibits a slow and nearly linear decline throughout the simulation period. In contrast, the controlled trajectory decreases more rapidly after the initial stage and continues to fall at a greater rate. The observed trends suggest that the proposed interventions not only promote smoking cessation but also reduce the incidence of asthma among non-smokers. Maintaining a larger ex-smoker population while simultaneously lowering respiratory complications indicates that long-term control strategies can substantially improve respiratory health and decrease the burden of smoking-related diseases.

Figure 18 illustrates the behaviour of smoker-related asthma populations $D_C(t)$ and $D_F(t)$. In Figure 18a, both trajectories begin at the same initial value and decrease over time. The controlled solution shows a steeper decline, particularly after the midpoint of the simulation, resulting in substantially fewer active smokers suffering from asthma. This outcome indicates that the control measures play an important role in reducing disease burden among current smokers. Similarly, Figure 18b presents the dynamics of $D_F(t)$. Although both solutions decrease gradually, the controlled trajectory falls much faster than the uncontrolled one. The results suggest that the combined control strategy not only reduces smoking prevalence but also contributes to improved health outcomes in individuals with a history of smoking. The reduction in asthma cases among both current and former smokers demonstrates that smoking cessation and continuous treatment remain beneficial even after prolonged smoking exposure. These results indicate that integrated intervention programmes can significantly reduce the prevalence of chronic respiratory diseases and improve long-term health outcomes.

Figure 19 shows the evolution of non-smokers and active-smokers affected by heart disease or high blood pressure, represented by $J_M(t)$ and $J_C(t)$, respectively. In Figure 19a, the uncontrolled trajectory decreases slowly over the entire simulation period. Under control measures, a brief initial rise is observed, followed by a sustained decline that becomes much steeper after the midpoint of the simulation. Figure 19b exhibits a similar trend for $J_C(t)$. Both curves decline over time, but the controlled trajectory decreases more rapidly and diverges progressively from the uncontrolled solution. The substantial reduction achieved under optimal control demonstrates the effectiveness of awareness and treatment efforts in lowering smoking-related cardiovascular risks among active smokers. The substantial decline in cardiovascular complications under the controlled scenario suggests that reducing smoking prevalence has a direct positive impact on cardiovascular health.

Figure 20 describes the dynamics of ex-smokers experiencing heart disease, denoted by $J_F(t)$. Both the controlled and uncontrolled trajectories display a downward trend throughout the simulation period. However, the decline under optimal control is considerably stronger, particularly after the middle of the time interval. The gap between the two solutions widens steadily, showing that the intervention significantly reduces cardiovascular complications among ex-smokers. By the end of the simulation, the controlled population reaches a much lower level than the uncontrolled case. The continued reduction in cardiovascular complications among ex-smokers indicates that the health benefits of smoking cessation extend well beyond quitting smoking. Early intervention and sustained treatment can substantially reduce the progression of smoking-related cardiovascular diseases and improve long-term clinical outcomes.

Figure 21 presents the optimal control profiles $\hbar_1(t)$ and $\hbar_2(t)$. In Figure 21a, the awareness control $\hbar_1(t)$ is applied intensively during the early stages of the simulation, where it exhibits several fluctuations before gradually decreasing to nearly zero. This behaviour suggests that awareness campaigns are most effective when implemented aggressively at the beginning of the intervention period. Figure 21b illustrates the treatment-related control $\hbar_2(t)$. The control remains relatively low during the initial phase but increases steadily as time progresses.

After approximately the midpoint of the simulation, $\hbar_2(t)$ rises rapidly and eventually reaches its maximum level, where it remains constant until the final time. This pattern indicates that treatment measures become increasingly important as the intervention progresses and are required at full intensity to achieve the greatest reduction in smoking-related health complications. The optimal control profiles suggest that awareness campaigns should be implemented intensively during the early stages of intervention to reduce smoking initiation, whereas treatment efforts should be strengthened progressively to manage existing smoking-related diseases. This coordinated strategy provides an effective balance between prevention and treatment, resulting in improved population health over time.

The numerical simulations clearly demonstrate that the optimal control strategy substantially improves the system dynamics. The implementation of awareness and treatment controls increases the populations of non-smokers and ex-smokers while reducing active smokers and the associated respiratory and cardiovascular disease classes. The results confirm that the combined control approach is effective in mitigating the adverse health consequences of smoking and contributes to a healthier population over time.

7. Conclusion

In order to explain the development of asthma and cardiovascular issues brought on by smoking behavior in a community, a thorough mathematical model was developed in this study. The analytical study verified that the model is both theoretically well-posed and biologically viable, guaranteeing positivity, boundedness, and the presence of solutions inside the non-negative orthant. In order to assess system stability, the baseline and positive equilibrium points were examined. The nonstandard finite difference (NSFD) scheme was used in numerical simulations to verify the analytical results. The numerical outcomes remained consistent with the theoretical analysis without generating numerical instabilities. The numerical results showed the increased fall of sick classes under controlled conditions and the natural growth of smoking-related health consequences when no interventions are implemented. The present NSFD formulation ensures the positivity and boundedness of all state variables for biologically feasible initial conditions. Moreover, the scheme preserves the qualitative dynamics of the continuous model without introducing numerical artifacts. Another significant advantage is its stability under relatively larger step sizes due to the nonstandard denominator function, which enhances computational efficiency. To assess the efficacy of two intervention strategies, treatment initiatives and awareness campaigns, an optimal control framework was incorporated into the model. Pontryagin's Maximum Principle was used to derive the optimality system, and simulations showed that applying both controls together greatly reduces the number of people with asthma and cardiovascular issues. Simultaneously, the treatments encourage a rise in non-smokers and ex-smokers, demonstrating the usefulness of these tactics in reducing the negative effects of smoking. Adopting both medical and public health measures concurrently is crucial for long-term disease reduction. At the same time, the controlled system promotes recovery and supports the growth of healthier population classes. The findings suggest that awareness-based interventions together with medical treatment strategies can play a significant role in reducing the long-term burden of asthma and cardiovascular diseases associated with smoking. Therefore, the model may assist health authorities and policymakers in designing effective prevention and intervention programs. Despite the significant insights this approach offers, there are also a number of drawbacks. The approach does not specifically account for variables that may affect asthma and cardiovascular outcomes, such as age structure, genetic vulnerability, or environmental pollution, and it assumes homogenous interactions across all groups. Although the proposed model is parameterized using hospital records, published literature, and survey-based behavioral data, future work will focus on incorporating parameter uncertainty analysis and statistical calibration using longitudinal epidemiological datasets to further improve the predictive capability of the model. Future developments might concentrate on using machine learning techniques for better parameter estimation and prediction accuracy or adding fractional-order derivatives, which more accurately represent memory effects. To gain a more thorough understanding of the dynamics of smoking-related health, future advancements may potentially incorporate stochastic variants, regional heterogeneity, or new control techniques like environmental regulation and tobacco taxation. Overall, the proposed framework provides a strong foundation for further investigations into smoking-associated disease transmission and control.

Data availability

The data supporting the findings of this study were generated through numerical simulations based on the proposed mathematical model and are included within the article. All data analyzed and generated during this study are included in this article.

Declaration of competing interest

The authors declare that they have no known competing financial interests or personal relationships that could have appeared to influence the work reported in this manuscript.

Funding

This research received no external funding.

References

[1] I. R. Sofia, S. R. Bandekar & M. Ghosh, "Mathematical modeling of smoking dynamics in society with impact of media information and awareness", Results in Control and Optimization **11** (2023) 100233. https://doi.org/10.1016/j.rico.2023.100233.

[2] M. Ghosh, "Industrial pollution and Asthma: a mathematical model", Journal of Biological Systems **8** (2000) 347. https://doi.org/10.1142/S0218339000000225.

[3] R. Polosa & N. C. Thomson, "Smoking and asthma: dangerous liaisons", European Respiratory Journal **41** (2013) 716. https://doi.org/10.1183/09031936.00073312.

[4] D. P. Strachan, "The role of environmental factors in asthma", British Medical Bulletin **56** (2000) 865. https://doi.org/10.1258/0007142001903562.

[5] A. J. Driscoll, S. H. Arshad, L. Bont, S. M. Brunwasser, T. Cherian, J. A. Englund, D. B. Fell, L. L. Hammitt, T. V. Hartert, B. L. Innis, R. A. Karron, G. E. Langley, E. K. Mulholland, P. K. Munywoki, H. Nair, J. R. Ortiz, D. A. Savitz, N. M. Scheltema, E. A. F. Simões, P. G. Smith & D. R. Feikin., "Does respiratory syncytial virus lower respiratory illness in early life cause recurrent wheeze of early childhood and asthma? Critical review of the evidence and guidance for future studies from a World Health Organization-sponsored meeting", Vaccine **38** (2020) 2435. https://doi.org/10.1016/j.vaccine.2020.01.020.

[6] Y. Riza, D. Adam, Y. Christina, A. Z. Anwary, Netty, E. Handayani, H. K. Inayah, A. Malik, Y. Oktaviani & A. Widyarni, "Public health policy in action: the impact of enforcing Local Regulation No. 7 of 2013 on smoke-free areas", Universal Journal of Public Health **13** (2025) 250. https://doi.org/10.13189/ujph.2025.130125.

[7] N. E. Collishaw, J. Kirkbride & D. T. Wigle, "Tobacco smoke in the workplace: an occupational health hazard", Canadian Medical Association Journal **131** (1984) 1199. Available online: https://pmc.ncbi.nlm.nih.gov/articles/PMC1483688/.

[8] D. W. Dockery, C. A. Pope, X. Xu, J. D. Spengler, J. H. Ware, M. E. Fay, B. G. Ferris Jr. & F. E. Speizer, "An association between air pollution and mortality in six US cities", New England Journal of Medicine **329** (1993) 1753. https://doi.org/10.1056/NEJM199312093292401.

[9] M. J. Utell & R. J. Looney, "Environmentally induced asthma", Toxicology Letters **82** (1995) 47. https://doi.org/10.1016/0378-4274(95)03467-6.

[10] R. Jan & Y. Xiao, "Effect of partial immunity on transmission dynamics of dengue disease with optimal control", Mathematical Methods in the Applied Sciences **42** (2019) 1967. https://doi.org/10.1002/mma.5491.

[11] Z. Hammouch & T. Mekkaoui, "Control of a new chaotic fractional-order system using Mittag-Leffler stability", Nonlinear Studies **22** (2015) 565. Available online: https://nonlinearstudies.com/index.php/nonlinear/article/view/1245.

[12] M. Sohaib, "Mathematical modeling and numerical simulation of HIV infection model", Results in Applied Mathematics **7** (2020) 100118. https://doi.org/10.1016/j.rinam.2020.100118.

[13] R. J. Attaullah & A. Jabeen, "Solution of the HIV infection model with full logistic proliferation and variable source term using Galerkin scheme", Matrix Science Mathematic **4** (2020) 37. https://www.researchgate.net/publication/349945043_Solution_of_The_Hiv_Infection_Model_With_Full_Logistic_Proliferation_and_Variable_Source_Term_Using_Galerkin_Scheme.

[14] R. Jan & Y. Xiao, "Effect of pulse vaccination on dynamics of dengue with periodic transmission functions", Advances in Difference Equations **2019** (2019) 368. https://doi.org/10.1186/s13662-019-2314-y.

[15] M. R. Mahmoudi, D. Baleanu, S. S. Band & A. Mosavi, "Factor analysis approach to classify COVID-19 datasets in several regions", Results in Physics **25** (2021) 104071. https://doi.org/10.1016/j.rinp.2021.104071.

[16] H. M. Baskonus, Z. Hammouch, T. Mekkaoui & H. Bulut, "Chaos in the fractional order logistic delay system: circuit realization and synchronization", in AIP Conference Proceedings, 1738 (2016) 290005. https://doi.org/10.1063/1.4952077.

[17] M. Slowikowska, J. Bajzert, J. Miller, T. Stefaniak & A. Niedźwiedź, "The dynamics of circulating immune complexes in horses with severe equine asthma", Animals **11** (2021) 1001. https://doi.org/10.3390/ani11041001.

[18] C. Castillo-Garsow, G. Jordan-Salivia & A. Rodriguez-Herrera, "Mathematical models for the dynamics of tobacco use, recovery and relapse", Biometrics Unit Technical Report BU-1505-M, Cornell University, Ithaca, USA, 1997. https://mcmsc.asu.edu/sites/g/files/litvpz576/files/2024-09/MTBI%201997%20Tobacco%20Use%20Report.pdf.

[19] O. Sharomi & A. B. Gumel, "Curtailing smoking dynamics: a mathematical modeling approach", Applied Mathematics and Computation **195** (2008) 475. https://doi.org/10.1016/j.amc.2007.05.012.

[20] V. Verma, "Optimal control analysis of a mathematical model on smoking", Modeling Earth Systems and Environment **6** (2020) 2535. https://doi.org/10.1007/s40808-020-00847-1.

[21] G. Zaman, Y. H. Kang & I. H. Jung, "Optimal treatment of an SIR epidemic model with time delay", BioSystems **98** (2009) 43. https://doi.org/10.1016/j.biosystems.2009.05.006.

[22] S. Lee, E. Jung & C. Castillo-Chavez, "Optimal control intervention strategies in low and high risk problem drinking populations", Socio-Economic Planning Sciences **44** (2010) 258. https://doi.org/10.1016/j.seps.2010.07.006.

[23] A. S. Devi, P. A. Naik, S. Boulaaras, N. Sene & Z. Huang. "Understanding the transmission mechanism of HIV/TB co-infection using fractional framework with optimal control", International Journal of Numerical Modelling: Electronic Networks, Devices and Fields **38** (2025) e70097. https://doi.org/10.1002/jnm.70097.

[24] P. A. Naik, B. M. Yeolekar, S. Qureshi, M. Yeolekar & A. Madzvamuse. "Modeling and analysis of the fractional-order epidemic model to investigate mutual influence in HIV/HCV co-infection", Nonlinear Dynamics **112** (2024) 11679. https://doi.org/10.1007/s11071-024-09653-1.

[25] O. Zakary, M. Rachik & I. Elmouki, "On the analysis of a multi-regions discrete SIR epidemic model: an optimal control approach", International Journal of Dynamics and Control **5** (2017) 917. https://doi.org/10.1007/s40435-016-0233-2.

[26] B. Khajji, A. Kouidere, O. Balatif & M. Rachik. "Mathematical modeling, analysis and optimal control of an alcohol drinking model with liver complication", Communications in Mathematical Biology and Neuroscience **2020** (2020) 32. https://doi.org/10.28919/cmbn/4553.

[27] B. Khajji, A. Labzai, A. Kouidere, O. Balatif & M. Rachik. "A discrete mathematical modeling of the influence of alcohol treatment centers on the drinking dynamics using optimal control", Journal of Applied Mathematics **2020** (2020) 9284698. https://doi.org/10.1155/2020/9284698.

[28] A. Omame & M. Abbas, "The stability analysis of a co-circulation model for COVID-19, dengue, and zika with nonlinear incidence rates and vaccination strategies", Healthcare Analytics **3** (2023) 100151. https://doi.org/10.1016/j.health.2023.100151.

[29] A. Omame & M. Abbas, "Modeling SARS-CoV-2 and HBV co-dynamics with optimal control", Physica A: Statistical Mechanics and its Applications **615** (2023) 128607. https://doi.org/10.1016/j.physa.2023.128607.

[30] A. Omame, M. Abbas & C. P. Onyenegecha. "Backward bifurcation and optimal control in a co-infection model for SARS-CoV-2 and ZIKV", Results in Physics **37** (2022) 105481. https://doi.org/10.1016/j.rinp.2022.105481.

[31] T. Faniran, A. Ali, M. O. Adewole, B. Adebo & O. O. Akanni. "Asymptotic behavior of tuberculosis between smokers and non-smokers", Partial Differential Equations in Applied Mathematics **5** (2022) 100244. https://doi.org/10.1016/j.padiff.2021.100244.

[32] A. Sharma & A. K. Misra, "Backward bifurcation in a smoking cessation model with media campaigns", Applied Mathematical Modelling **39** (2015) 1087. https://doi.org/10.1016/j.apm.2014.07.022.

[33] I. R. Sofia & M. Ghosh, "Mathematical modeling of smoking habits in the society", Stochastic Analysis and Applications **41** (2023) 918. https://doi.org/10.1080/07362994.2022.2093223.

[34] A. Labzai, O. Balatif & M. Rachik. "Optimal control strategy for a discrete time smoking model with specific saturated incidence rate", Discrete Dynamics in Nature and Society **2018** (2018) 5949303. https://doi.org/10.1155/2018/5949303.

[35] S. Musa, S. M. Ahmad & H. B. Aliyu, "Impact of health education campaign on the dynamics of cigarette smoking in a varying population", Dutse Journal of Pure and Applied Sciences **5** (2019) 141.

[36] S. S. Alzaid & B. S. T. Alkahtani, "Asymptotic analysis of a giving up smoking model with relapse and harmonic mean type incidence rate", Results in Physics **28** (2021) 104437. https://doi.org/10.1016/j.rinp.2021.104437.

[37] O. Khyar, J. Danane & K. Allali. "Mathematical analysis and optimal control of giving up the smoking model", International Journal of Differential Equations **2021** (2021) 8673020. https://doi.org/10.1155/2021/8673020.

[38] M. Farman, N. Asghar, M. U. Saleem, K. S. Nisar, K. Hosseini & M. Hafez. "Predictive and global effect of active smoker in asthma dynamics with Caputo fractional derivative", Computer Modeling in Engineering & Sciences **145** (2025) 721. https://doi.org/10.32604/cmes.2025.069541.

[39] M. Farman, N. Asghar, M. U. Saleem, S. Salahshour, A. Smerat & M. Hafez. "Optimal control and dynamical transmission of asthma due to smoking populations: incorporating medical and public health measures", Results in Control and Optimization **22** (2026) 100674. https://doi.org/10.1016/j.rico.2026.100674.

[40] R. Anguelov & J. M. S. Lubuma, "Contributions to the mathematics of the nonstandard finite difference method and applications", Numerical Methods for Partial Differential Equations **17** (2001) 518. https://doi.org/10.1002/num.1025.

[41] R. E. Mickens (Ed.), *Nonstandard finite difference models of differential equations*, World Scientific, Singapore, 1993, pp. 68-92. https://doi.org/10.1142/9789814440882_0003.

[42] J. M. S. Lubuma & K. C. Patidar, "Non-standard methods for singularly perturbed problems possessing oscillatory/layer solutions", Applied Mathematics and Computation **187** (2007) 1147. https://doi.org/10.1016/j.amc.2006.09.011.

[43] A. B. Gumel (Ed.), Mathematics of Continuous and Discrete Dynamical Systems, Contemporary Mathematics Series, Vol. 618, American Mathematical Society, Providence, Rhode Island, USA, 2014. Available online: https://bookstore.ams.org/conm-618.

[44] M. McAsey, L. Mou & W. Han "Convergence of the forward-backward sweep method in optimal control", Computational Optimization and Applications **53** (2012) 207. https://doi.org/10.1007/s10589-011-9454-7.

[45] C. L. Hwang & L. T. Fan, "A discrete version of Pontryagin's maximum principle", Operations Research **15** (1967) 139. https://doi.org/10.1287/opre.15.1.139.

[46] V. Guibout & A. Bloch, "A discrete maximum principle for solving optimal control problems", in Proceedings of the 43rd IEEE Conference on Decision and Control (CDC), IEEE, Bahamas (2004), pp. 1806–1811. https://ieeexplore.ieee.org/document/1430309.

[47] L. S. Pontryagin, *Mathematical theory of optimal processes*, Routledge, London, 2018. https://www.taylorfrancis.com/books/mono/10.1201/9780203749319/mathematical-theory-optimal-processes-pontryagin.

[48] E. Todorov & M. I. Jordan, "Optimal feedback control as a theory of motor coordination", Nature Neuroscience **5** (2002) 1226. https://doi.org/10.1038/nn963.